ISSN 0016-7029, Geochemistry International, 2007, Vol. 45, No. 12, pp. 1210–1234. © Pleiades Publishing, Ltd., 2007.
Original Russian Text © P.Ya. Azimov, S.A. Bushmin, 2007, published in Geokhimiya, 2007, No. 12, pp. 1305–1330.

Solubility of Minerals of Metamorphic and Metasomatic Rocks in Hydrothermal Solutions of Varying Acidity: Thermodynamic Modeling at 400–800°C and 1–5 kbar

P. Ya. Azimov and S. A. Bushmin

Institute of Precambrian Geology and Geochronology, Russian Academy of Sciences, nab. Makarova 2, St. Petersburg, 199034 Russia

e-mail: az@pa1400.spb.edu

Received June 6, 2005

Abstract—The character of solubility of 61 metamorphic and metasomatic minerals in an aqueous fluid was analyzed as a function of temperature, pressure, and fluid acidity by means of computer simulation of mineral–fluid equilibria. Depending on the behavior of minerals in solutions of varying acidity, six main types of solubility diagrams were distinguished. The solubility of the majority of minerals is controlled mainly by fluid acidity rather than by *P–T* conditions. The analysis of model results provided insight into the mobility of chemical elements composing the minerals. The highest mobility in solutions of any acidity was established for Si, K, and Na. Ca and Mg are mobile in acidic solutions and inert in neutral and alkaline solutions. Fe(II) and Mn(II) are mobile in acidic and alkaline solutions but inert in neutral solutions. Fe(III) is mobile only in strongly acidic solutions and practically immobile in solutions of other compositions, which suggests that ferrous iron species must prevail in solutions. Al is mobile in alkaline and ultra-acidic solutions but inert in neutral and slightly acidic solutions. Correspondingly, a change in acidity must lead to the migration of some component into the solution and precipitation of other components. These conclusions are in agreement with the sequences of element mobility deduced from the experimental investigation of metasomatism. Most metamorphic fluids must be rich in silica and alkalis, which may result in the appearance of aggressive silica–alkali fluids responsible for regional metasomatism and granitization. In general, the solubility of Fe-, Mg-, Mn-, and Ca-bearing minerals in alkaline solutions is low compared with acidic solutions. Therefore, only acidic initial solutions could produce fluids enriched in these elements at the expense of leaching from metamorphic rocks during fluid migration. Fluids enriched mainly in Fe could initially be both acidic and alkaline.

DOI: 10.1134/S0016702907120038

1. INTRODUCTION

The investigation of mineral solubility in hydrothermal solutions over a wide range of temperature and pressure provides a necessary basis for the subsequent analysis of metamorphic, metasomatic, and ore-forming processes. Together with the initial compositions of interacting fluid and rocks, the solubility of minerals controls the composition of equilibrium fluid [1–4]. The values of solubility can be determined in two ways. The first and most robust approach is the direct experimental investigation of saturated solutions. However, the experimental determination of mineral solubility in a wide range of parameters of state is technically difficult, and such investigations are scarce and do not embrace the whole temperature–pressure field corresponding to the conditions of metamorphic and postmagmatic mineral formation and the possible range of fluid compositions. Moreover, experimental modeling is complicated by the problems in attaining equilibrium during mineral dissolution.

The second approach allows considering a wide range of mineral formation conditions, including the fields inaccessible for direct experimental modeling, and makes use of thermodynamic computer modeling on the basis of the principles of chemical thermodynamics. The theoretical prediction of mineral solubility can be regarded as the main method of study for those areas of high temperatures, pressures, and fluid compositions where experiments are currently limited or impracticable. In addition, modern analytical methods do not allow determination of fluid acidity and ionic composition at high pressures and temperatures without disturbing the established equilibrium.

2. CONDITIONS AND METHODS OF THERMODYNAMIC CALCULATIONS

The solubility of 61 minerals was analyzed in the system Na_2O–K_2O–CaO–FeO–MgO–MnO–Al_2O_3–Fe_2O_3–SiO_2–H_2O (table). Among them are oxides, hydroxides, and silicates widespread in metamorphic and metasomatic rocks. The solubility of carbonates, ore, and accessory minerals and solid solutions is not addressed in this paper. The solubility was investigated by the method of the computer simulation of mineral–

Classification of minerals of metamorphic and metasomatic rocks with respect to the type of solubility diagram

Mineral	Symbol	Formula	Mineral	Symbol	Formula
Type 1			Zoisite	*Zo*	$Ca_2Al_3(SiO_4)(Si_2O_7)OOH$
Quartz	*Qtz*	SiO_2	Epidote	*Ep*	$Ca_2Al_2Fe(SiO_4)(Si_2O_7)OOH$
Jadeite	*Jd*	$NaAlSi_2O_6$	Actinolite	*Act*	$Ca_2Fe_5(Si_8O_{22})(OH)_2$
Albite	*Ab*	$NaAlSi_3O_8$	Amesite	*Ams*	$Mg_4Al_2(Al_2Si_2O_{10})(OH)_8$
Microcline	*Mi*	$KAlSi_3O_8$	Rhodonite	*Rdn*	$MnSiO_3$
Type 2			**Type 5**		
Muscovite	*Ms*	$KAl_2(AlSi_3O_{10})(OH)_2$	Pyrope	*Prp*	$Mg_3Al_2(SiO_4)_3$
Paragonite	*Pg*	$NaAl_2(AlSi_3O_{10})(OH)_2$	Andradite	*Adr*	$Ca_3Fe_2(SiO_4)_3$
Andalusite	*And*	Al_2SiO_3	Grossular	*Grs*	$Ca_3Al_2(SiO_4)_3$
Kyanite	*Ky*	Al_2SiO_5	Hedenbergite	*Hed*	$CaFe(Si_2O_6)$
Sillimanite	*Sil*	Al_2SiO_5	Tschermakite	*Ts*	$Ca_2(Mg_3Al_2)(Al_2Si_6O_{22})(OH)_2$
Corundum	*Cor*	$A1_2O_3$	Vesuvianite	*Ves*	$Ca_{19}Mg_2Al_{11}(SiO_4)_{12}(Si_2O_7)_3(OH)_9$
Hematite	*Hem*	Fe_2O_3	Clinochlore	*Ccl*	$Mg_5Al(AlSi_3O_{10})(OH)_8$
Type 3			Prehnite	*Prh*	$Ca_2Al(AlSi_3O_{10})(OH)_2$
Almandine	*Alm*	$Fe_3Al_2(SiO_4)_3$	Riebeckite	*Rbk*	$Na_2Fe_3Fe_2(Si_8O_{22})(OH)_2$
Spessartine	*Sps*	$Mn_3Al_2(SiO_4)_3$	Gedrite	*Ged*	$Mg_5Al_2(Si_6Al_2O_{22})(OH)_2$
Staurolite	*St*	$Fe_4Al_{18}(SiO_4)_{7.5}O_{14}(OH)_4$	**Type 6**		
Mg-staurolite	*mSt*	$Mg_4Al_{18}(SiO_4)_{7.5}O_{14}(OH)_4$	Phlogopite	*Phl*	$KMg_3(AlSi_3O_{10})(OH)_2$
Cordierite	*Crd*	$Mg_2Al_3(AlSi_5O_{18})$	Pargasite	*Pgs*	$NaCa_2Mg_4Al(Al_2Si_6O_{22})(OH)_2$
Fe-cordierite	*fCd*	$Fe_2Al_3(AlSi_5O_{18})$	Glaucophane	*Gln*	$Na_2Mg_3Al_2(Si_8O_{22})(OH)_2$
Chamosite	*Cha*	$Fe_5Al(AlSi_3O_{10})(OH)_8$	Aegirine	*Aeg*	$NaFe(Si_2O_6)$
Chloritoid	*Cld*	$FeAl_2(SiO_4)O(OH)_2$	Forsterite	*Fo*	$Mg_2(SiO_4)$
Fayalite	*Fa*	$Fe_2(SiO_4)$	Enstatite	*En*	$Mg_2(Si_2O_6)$
Ferrosilite	*Fs*	$Fe_2(Si_2O_6)$	Clinohumite	*Chu*	$Mg_9(SiO_4)_4(OH)_2$
Grunerit	*Gru*	$Fe_7(Si_8O_{22})(OH)_2$	Anthophyllite	*Ath*	$Mg_7(Si_8O_{22})(OH)_2$
Hercynite	*Hc*	$FeAl_2O_4$	Cummingtonite	*Cum*	$Mg_7(Si_8O_{22})(OH)_2$
Spinel	*Spl*	$MgAl_2O_4$	Chrysotile	*Ctl*	$Mg_3Si_2O_5(OH)_4$
Magnetite	*Mag*	$FeFe_2O_4$	Talc	*Tlc*	$Mg_3(Si_4O_{10})(OH)_2$
Sapphirine	*Spr442*	$Mg_4Al_4(Si_2Al_4O_{20})$	Diopside	*Di*	$CaMgSi_2O_6$
	Spr793	$Mg_{3.5}Al_{4.5}(Si_{1.5}Al_{4.5}O_{20})$	Tremolite	*Trm*	$Ca_2Mg_5(Si_8O_{22})(OH)_2$
Annite	*Ann*	$KFe_3(AlSi_3O_{10})(OH)_2$	Wollastonite	*Wo*	$CaSiO_3$
Type 4			Periclase	*Per*	MgO
Anorthite	*An*	$CaAl_2Si_2O_8$	Brucite	*Brc*	$Mg(OH)_2$
Lawsonite	*Lws*	$CaAl_2(Si_2O_7)(OH)_2 \cdot H_2O$	Portlandite	*Ptd*	$Ca(OH)_2$

aqueous fluid equilibria using the FLUID [5, 6] and GBFLOW [7] programs at temperatures of 400–800°C and pressures of 1, 3, and 5 kbar. The properties of water were calculated on the basis of the Haar–Gallagher–Kell model [8], and the properties of aqueous species were determined using the modified HKF model [9, 10]. Since the HKF model is valid only for aqueous fluids with a density of no less than 0.35 g/cm^3, calculations for a pressure of 1 kbar were conducted at 400–600°C only. Another limitation of the HKF model is that the properties of dissolved species cannot be calculated at pressures higher than 5 kbar, which hampered the analysis of mineral solubility at high pressures. The solubility of minerals was calculated for a pure water fluid and aqueous solutions containing acidic (HCl) or alkaline (NaOH) components. The concentrations of substances in solutions and the results of solubility computations are given in this paper in moles of dissolved substances per one kilogram of water and expressed in molality units (for instance, 0.1 M HCl corresponds to a solution containing 0.1 mole HCl per one kilogram H_2O).

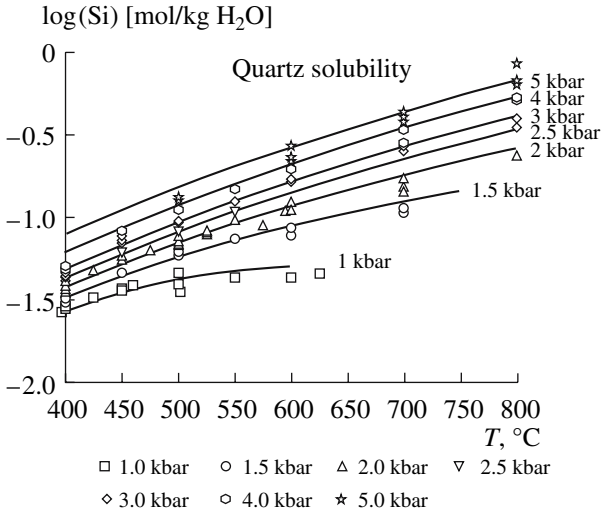

Fig. 1. Solubility of quartz in water at temperatures of 400–800°C and pressures of 1–5 kbar. The symbols denote the values of quartz solubility reported in [18–32], and the curves show calculated quartz solubility under various temperature and pressure conditions.

The thermodynamic properties of minerals were taken from the database of Holland and Powell [11], except for portlandite, $Ca(OH)_2$, the parameters of which were adopted from the UNITHERM 3.7 database [12]. The coefficients of the HKF equation of state were taken from the slop98.dat database as of October 30.1998 [13] for the following aqueous species: H^+, OH^-, Cl^-, SiO_2^0 (equivalent to $Si(OH)_4^0$), $HSiO_3^-$, Fe^{3+}, $FeOH^{2+}$, FeO^+ (equivalent to $Fe(OH)_2^+$), $HFeO_2^0$ (equivalent to $Fe(OH)_3^0$), FeO_2^- (equivalent to $Fe(OH)_4^-$), Fe^{2+}, $FeOH^+$, FeO^0 (equivalent to $Fe(OH)_2^0$), $HFeO_2^-$ (equivalent to $Fe(OH)_3^-$), $FeCl^{2+}$, $FeCl_2^0$, $FeCl^+$, Mg^{2+}, $MgOH^+$, $MgHSiO_3^+$, $MgCl^+$, Ca^{2+}, $CaOH^+$, $CaHSiO_3^+$, $CaCl_2^0$, $CaCl^+$, Na^+, $NaHSiO_3^0$, $NaCl^0$, and K^+. The data of Pokrovskii and Helgeson [14] were used for the species Al^{3+}, $AlOH^{2+}$, $Al(OH)_2^+$, $HAlO_2^0$ (equivalent to $Al(OH)_3^0$), AlO_2^- (equivalent to $Al(OH)_3^-$), $NaAlO_2^0$ (equivalent to $NaAl(OH)_4^0$), $KAlO_2^0$ (equivalent to $KAl(OH)_4^0$), $NaOH^0$, and KOH^0. The data of different authors for species in the Al–O–H system will be compared in detail during the discussion of experimental and model values for corundum solubility. The properties of $AlH_3SiO_4^{2+}$ were taken from [15], and those of the neutral HCl^0 and KCl^0 species, from [16] and [17], respectively.

3. COMPARISON OF THE RESULTS OF NUMERICAL SIMULATION WITH EXPERIMENTAL DATA ON MINERAL SOLUBILITY

For the analysis of the plausibility of thermodynamic modeling, the results of solubility calculations were compared with published experimental data. The potentialities of such a comparison are strongly limited by the fact that experimental data are available for the solubility of a few minerals within a narrow range of conditions. Most of these data are restricted to subcritical conditions and are not considered here. In this paper, we limited ourselves to the analysis of data at temperatures of higher than 400°C and pressures from 1 to 5 kbar.

There are other circumstances limiting the use of experimental solubility data. Equilibrium is not always attained in experiments, often owing to kinetic factors. Incomplete data were reported in many studies (for instance, only equilibrium SiO_2 concentrations in fluid are given for minerals of complex composition). In some cases, the format of solubility data does not allow their unambiguous recalculation to molalities. Natural minerals were often used in experiments, and admixture components could substantially affect the composition of solution.

3.1. Quartz Solubility

Quartz solubility has undoubtedly been studied most extensively. Quartz solubility data are available for a wide range of conditions. A high degree of knowledge is related to both the importance for the understanding of hydrothermal processes and relatively high quartz solubility, which facilitates experiments and allows the high-accuracy determination of solution composition. The experimental values of quartz solubility in water are compared with the results of our calculations in Fig. 1. The experimental and calculated values show adequate agreement, which is related to the good calibration of thermodynamic data for the aqueous species SiO_2^0 (equivalent to $Si(OH)_4^0$), which is predominant in the solution.

3.2. Corundum Solubility

Corundum is the next best studied mineral with respect to solubility in supercritical fluids. However, in contrast to quartz, experimental data on corundum solubility show a rather wide scatter (Fig. 2). This is caused by the low solubility of corundum resulting in a poor accuracy of the determination of aluminum concentration in solution and slow equilibration rates.

The calculated values of corundum solubility at various pressures are compared with experimental measurements in Fig. 3. It can be seen that the low-pressure (1.0–2.5 kbar) experimental data can be subdivided into two groups: data of (1) [33, 34, 38] and (2) [30, 35–37].

At pressures of ≥3 kbar, only data from group 2 studies are available. The calculations were based on the parameters of Al–O–H aqueous species in the HKF format from [14, 39] and from the slop98.dat database [13, 40]. As can be seen from the diagram, the calculations with these two sets of parameters yielded significantly different results. The values calculated using the parameters of Pokrovskii and Helgeson [14] for hydrous aluminum complexes are in agreement with the experimental data of the second group, especially at pressures above 2 kbar, whereas the results obtained using the properties of solution species from the slop98.dat database, Tagirov and Schott [39], and Shock et al. [40] are significantly different from any experimental data. Such a behavior of model solubility values is related to the fact that Pokrovskii and Helgeson derived the properties of aqueous species using thermodynamic data and solubility measurements under both subcritical and supercritical conditions, whereas Tagirov and Schott [39, 40] and Shock et al. [13, 40] used only data for subcritical temperatures and pressures. Because of this, the thermodynamic properties of aluminum hydroxy complexes after Pokrovskii and Helgeson were considered as adequate and were used in subsequent calculations.

3.3. Solubility of Aluminum Silicates

There is extensive experimental evidence for the incongruent dissolution of aluminum silicates (kyanite, andalusite, and sillimanite) with the preferential transfer of silica into the solution and precipitation of alumina (corundum). This is explained by the considerably different solubilities of SiO_2 and Al_2O_3 in aqueous solutions (cf. Figs. 1 and 2). The experimental data on the incongruent solubility of aluminum silicates are compared in Fig. 4 with the results of our calculations obtained using the properties of Al–O–H species from [14]. Also shown in Fig. 4 are the compositions of solutions in equilibrium with the andalusite + corundum assemblage, because this assemblage is produced by the incongruent dissolution of andalusite under the conditions of interest. The concentrations of SiO_2 in the solution are used for comparison, because the concentrations of Al_2O_3 were not determined in the majority of studies from which the data were taken, and in other studies they were determined with high errors because of their low magnitudes. The diagram illustrates a considerable scatter in the experimental data. The results of calculations are in agreement with the data on kyanite and andalusite solubility reported by Brown and Fyfe [41], especially at temperatures of higher than 500°C, and with the maximum values of kyanite solubility obtained in [43]. In all other cases, the experimental values are lower than calculated ones and lower than those from the experiments of Brown and Fyfe. This discrepancy is probably related to the incomplete equilibration in the experiments. The difficulties in attaining equilibrium are clearly illustrated by the scatter in

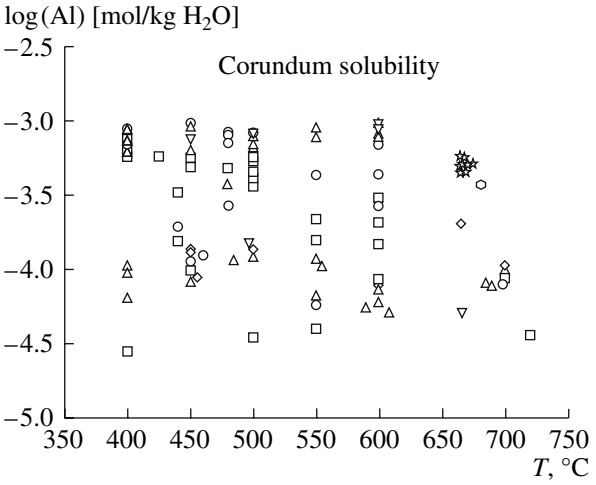

Fig. 2. Experimental data on corundum solubility in water at temperatures of 400–800°C and pressures of 1–5 kbar [30, 33–38]. Symbols are the same as in Fig. 1.

experimental data, especially in the experiments of Ostapenko and Arapova [43] and Ostapenko et al. [44].

3.4. Solubility of Alkali Aluminosilicates

The solubility of feldspars in water under supercritical parameters has been experimentally studied by a number of authors [28, 32, 45–49], but the values reported by them vary significantly for several reasons. First, this is related to the use of natural minerals in experiments. Even a small admixture of albite component in microcline results in a significant enrichment of sodium in aqueous solution [28], which affects the total solubility. Second, equilibrium was not reached in many experiments [28, 47]. The degree of equilibration is difficult to control, because the equilibrium was approached from one side in most experiments (dissolution of minerals in undersaturated solutions). Difficulty in the nucleation of new phases during incongruent dissolution can impede the attainment of equilibrium. In addition, the incompleteness of data in experimental papers may hamper their correct recalculation.

The incongruent dissolution of feldspars in pure water is their important feature; in contrast to aluminum silicates, different hydrolysis products are possible: white micas, aluminum silicates, corundum, leucite, and nepheline. This circumstance contributes to the uncertainty of solubility data. Unfortunately, most authors did not indicate which new phases were formed during the incongruent dissolution of feldspars. Data on fluid compositions are absent in some studies. For instance, only weight-loss values were reported in [32, 48] for experiments on albite dissolution. Taking into account that these authors mentioned the incongruent character of dissolution in their experiments, only apparent rather than true solubility can be correctly

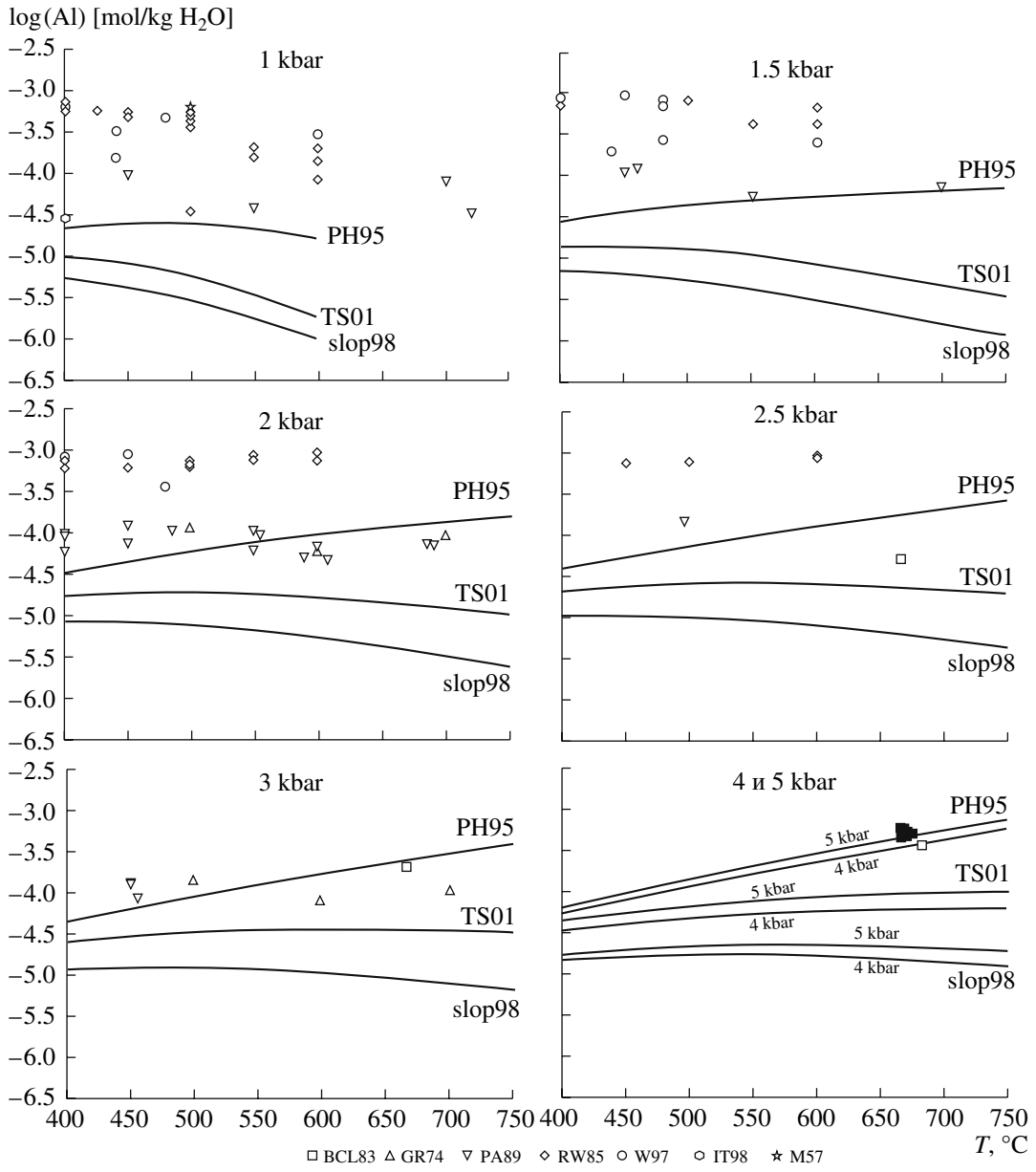

Fig. 3. Experimental and calculated values of corundum solubility in a water fluid. The symbols denote experimental data of various authors: IT98 [30], M57 [33], GR74 [34], BCL83 [35], RW85 [36], PA89 [37], and W97 [38]; the curves show the calculated solubility values based on the parameters of aqueous species of the Al–O–H system from [14] (PH95), [39] (TS01), and the slop98.dat database as of October 30, 1998 [13, 40].

derived from their data. Adcock [28] and Currie [47] observed the appearance of nepheline during albite dissolution, which is not consistent with the reported stoichiometric relations of components in the solution. These shortcomings strongly limit the possibility of comparison of the results of theoretical modeling with the experimental measurements of feldspar solubility.

Figure 5 shows the experimental measurements of potassium feldspar solubility compared with the calculated curves for congruent and incongruent solubility (the latter was computed taking into account the possible formation of leucite, muscovite, andalusite, and corundum). It can be seen from these diagrams that the experimental data are in better agreement with the curves of congruent rather than incongruent dissolution.

The situation is simpler in the case of three-mineral assemblages, which buffer the composition of solution in the Na_2O–Al_2O_3–SiO_2–H_2O and K_2O–Al_2O_3–SiO_2–H_2O systems. The kinetics of equilibration in such systems is independent of the nucleation of new phases, and the probability that the composition of solution determined in experiments corresponds to the equilibrium composition is higher in such a case. In addition,

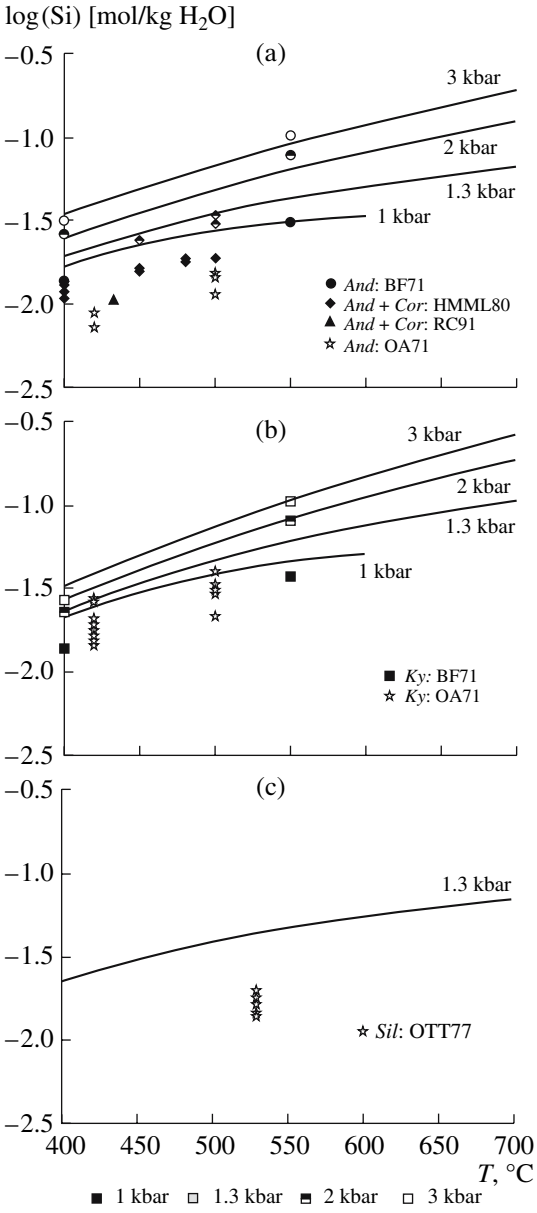

Fig. 4. Incongruent dissolution of (a) andalusite, (b) kyanite, and (c) sillimanite in water under supercritical conditions (400–700°C and 1–3 kbar). Sources of experimental data: BF71 [41], HMML80 [25], RC91 [42], OA71 [43], and OTT77 [44]. The curves show calculated equilibrium Si contents in fluid under various pressures. Mineral symbols in the diagrams and text are given in the table.

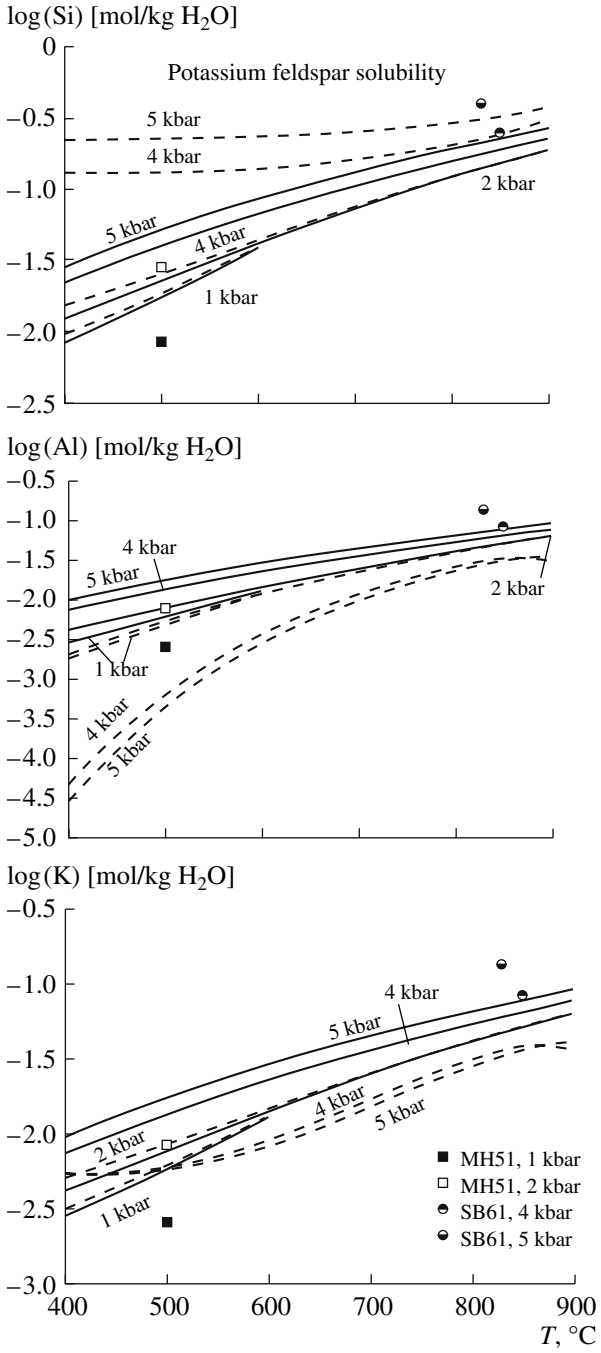

Fig. 5. Solubility of potassium feldspar in water at temperatures of 400–900°C and pressures of 1–5 kbar. The experimental data are after [45] (MH51) and [46] (SB61). The curves show the solubility of microcline calculated in this study; congruent and incongruent solubility curves are shown by solid and dashed lines, respectively.

the uncertainty in the phase assemblage is eliminated. Figure 6 shows the experimental and calculated compositions of solutions in equilibrium with the albite + paragonite + quartz assemblage. The experimental data are in rather good agreement with the results of the calculation. Adequate agreement was also observed for the potassium feldspar + muscovite + quartz assemblage (Fig. 7). Only the results of Anderson et al. [51] were used, whereas the solubility values reported for the same assemblage by Walther and Woodland [52] were ignored, because the concentration of Na in solution was similar to that of K or even higher in these experiments, despite the strong prevalence of K over Na in microcline (K/Na = 22) and muscovite (K/Na = 13). In such a case, equilibria between solid and aqueous solu-

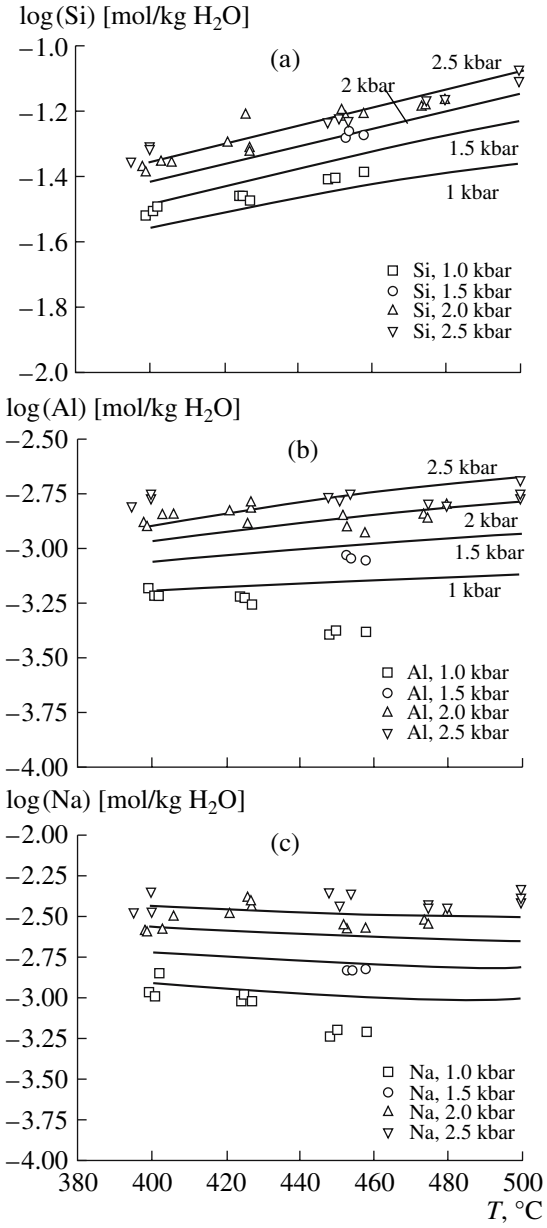

Fig. 6. Composition of solution in equilibrium with the albite + paragonite + quartz assemblage (Na_2O–Al_2O_3–SiO_2–H_2O system). The experimental data are after [50], and the curves show the calculated equilibrium compositions of solutions obtained in this study.

tions must be analyzed [53], which is beyond the scope of the present study.

3.5. Solubility of Magnesium and Calcium Minerals

Figure 8 shows the solubilities of magnesium and calcium hydroxides (brucite and portlandite) reported in [54] in comparison with theoretical calculations. It can be seen from this diagram that fairly good agreement is obtained for portlandite at pressures of 2–3 kbar, but the discrepancy increases with decreasing pressure

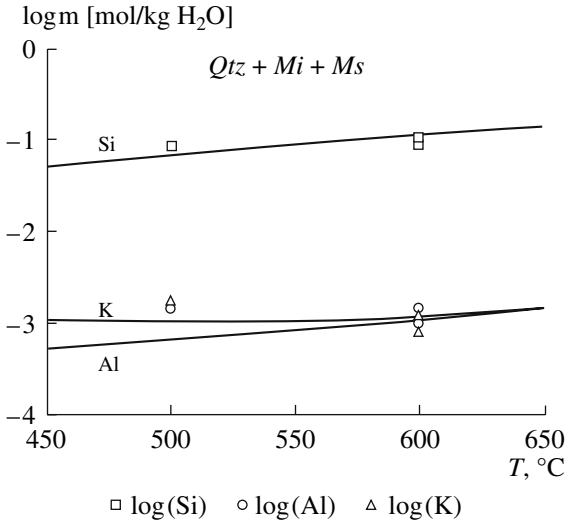

Fig. 7. Composition of solution in equilibrium with the potassium feldspar + muscovite + quartz assemblage (K_2O–Al_2O_3–SiO_2–H_2O system). The experimental data are after [51], and the curves show the calculated equilibrium compositions of solution obtained in this study.

and increasing temperature, i.e., with decreasing fluid density (calculated values are overestimated). In contrast, the theoretical values for brucite approach the experimental measurements at low pressures (less than 2 kbar) and high temperatures (above 500°C), and the difference between the calculated and experimental values increases with increasing pressure. However, if the solubility curves of periclase (MgO) are plotted in the same diagram, the experimental values of brucite solubility appear to be close to the calculated solubility of periclase. This fact is difficult to explain, because the approach to equilibrium from different directions was employed in the experiments of Walther [54]. However, the discrepancy is not so high as to consider the thermodynamic properties of the aqueous species of Ca and Mg as inappropriate for calculations.

Figure 9 shows the concentrations of SiO_2 in aqueous fluid in equilibrium with the two-mineral assemblages talc + chrysotile, talc + forsterite [55], and enstatite + forsterite [56], which buffer the content of silica in the equilibrium fluid, and the results of numerical calculations for these values. In this case, the measured values are in adequate agreement with the theoretical estimates. This is related to the fact that the result of calculations for such buffer equilibria is primarily controlled by the thermodynamic properties of minerals, which are rather reliably constrained, and the properties of the SiO_2^0 species, which are also well known, as was shown above. The properties of magnesium species do not affect the results of calculations for equilibrium silica concentrations owing to their low concentrations in the solutions of the MgO–SiO_2–H_2O system.

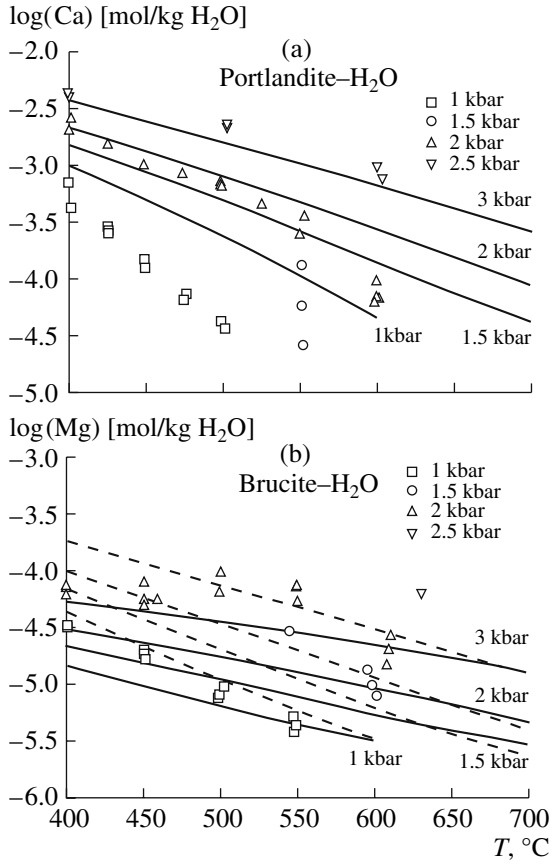

Fig. 8. Solubility of portlandite $Ca(OH)_2$ and brucite $Mg(OH)_2$ in a supercritical water solution. The experimental data on mineral solubility are after [54]. The solid lines show the equilibrium values of portlandite and brucite solubility, and the dashed curves denote the calculated solubility of periclase, MgO.

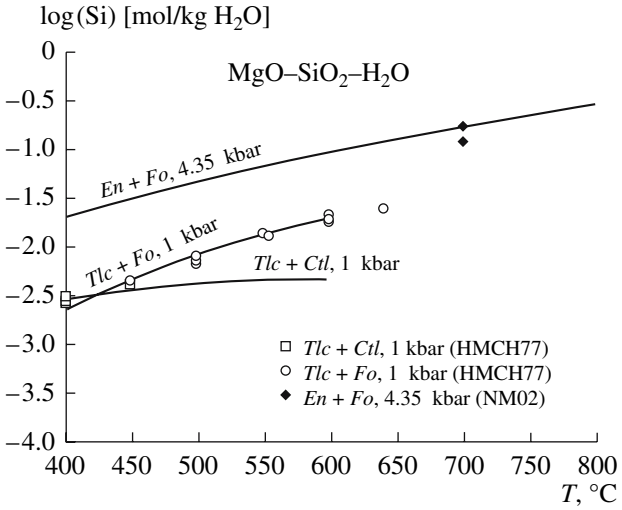

Fig. 9. Concentrations of SiO_2 in supercritical fluids in equilibrium with buffer assemblages in the $MgO–SiO_2–H_2O$ system. The experimental data are after [55] for the *Tlc* + *Ctl* and *Tlc* + *Fo* assemblages and after [56] for the *En* + *Fo* assemblage. The curves show the equilibrium compositions of solutions calculated in this study.

In contrast, the experimental data on the solubility of enstatite [45] are significantly different from the calculated values (Fig. 10). They fall between the calculated equilibrium concentrations of magnesium and silica for incongruent dissolution and are higher than the concentrations estimated for congruent dissolution. This could be due to incomplete equilibration, because the difference between the concentrations of magnesium and silicon determined by Morey and Hesselgesser [45] is rather small and must presumably be higher. Moreover, it was shown above that the solubilities of brucite and quartz are adequately described under the given conditions (600°C and 1 kbar).

Shmulovich et al. [32] reported only weight-loss measurements for the dissolution of diopside and albite but did not determine the compositions of solution, despite the strongly incongruent character of dissolution. Therefore, their data cannot be used for comparison.

The above analysis showed that the modified HKF model and the available thermodynamic parameters of aqueous species in the format of this model can be used to simulate the solubility of minerals in supercritical aqueous solutions. Of course, both the model and, especially, the properties of aqueous species require further refinement, and the set of minerals and complexes that can be used for calculations should be extended. We caution against the use of parameters derived from solubility data obtained under subcritical parameters, especially at temperatures of lower than 100°C, to simulate equilibria involving supercritical fluid.

4. TOPOLOGY OF SOLUBILITY DIAGRAMS

In order to evaluate the behavior of minerals in aqueous fluids, the solubility of minerals in aqueous fluids was calculated under various *P–T* and acidity–alkalinity conditions. The acidity of aqueous fluid was constrained during modeling by the concentrations of HCl and NaOH. The calculations showed that variations in acidity exert a much greater influence on the solubility of the majority of minerals than changes in temperature and pressure. The analysis of solubility diagrams as a function of the acidity–alkalinity of fluid allowed us to distinguish six major types of such dependencies (Fig. 11). These types are described below together with general features in the behavior of minerals in aqueous fluids depending on dissolution conditions.

4.1. Character of Mineral Dissolution

Minerals of complex composition (consisting of three or more elements) usually dissolve incongruently. The dissolution proper is then accompanied by the crystallization of one or several new minerals. Thus, incongruent dissolution is a complex reaction, which can be described as a series of simple (congruent) reac-

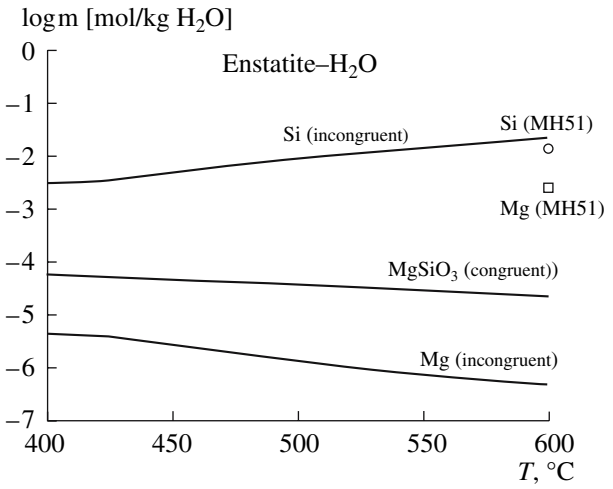

Fig. 10. Solubility of enstatite in a supercritical water fluid. The experimental data for enstatite are after [45]. The curves show the calculated concentrations of elements in the fluid for the congruent and incongruent dissolution of enstatite. The incongruent dissolution of enstatite produces the *Tlc* + *Ctl* assemblage at 400°C and *Tlc* + *Fo* at higher temperatures (Fig. 9).

tions. The congruent or incongruent character of mineral dissolution depends on a number of conditions, including the compositions of the mineral assemblage and fluid. For instance, aluminum silicates, andalusite, kyanite, and sillimanite, dissolve incongruently with the formation of corundum, but their dissolution becomes congruent in the presence of excess silica (quartz). Congruent dissolution is also possible in the limiting case of a completely open system, when all the dissolved components are removed from the zone of mineral dissolution. Such a behavior was experimentally reproduced by Vidal and Durin [57]. Our study focuses on the behavior of particular minerals rather than mineral assemblages, and only congruent dissolution will be considered during the analysis of solubility diagrams.

4.2. Types of Diagrams of Congruent Dissolution

Type 1. Solubility diagrams of the first type (Fig. 11) are characteristic of quartz and alkali–aluminum silicates: jadeite, microcline, and albite. These minerals show high solubilities (more than 10^{-2}–10^{-3} mol/kg H_2O), which are almost independent of the acidity of the medium (Fig. 12). As pressure increases from 1 to 5 kbar, the solubility of minerals of this type increases by approximately half an order of magnitude (one order of magnitude in the case of quartz). The solubility also increases by approximately an order of magnitude with a temperature increase from 400 to 800°C. The sequence of the solubility of type 1 minerals in pure water is shown in Fig. 16. With increasing pressure, albite may become slightly more soluble than microcline, but in general these phases have similar solubilities.

Type 2. The second type of solubility diagrams (Fig. 11) is characteristic of aluminous minerals: white micas (muscovite and paragonite), aluminum silicates (andalusite, kyanite, and sillimanite), and oxides of Al (corundum) and Fe(III) (hematite). These minerals are less soluble than the minerals of the first group. Micas are most soluble among them, while corundum and, especially, hematite show the lowest solubility (Fig. 16). The minerals of this type show the lowest solubility

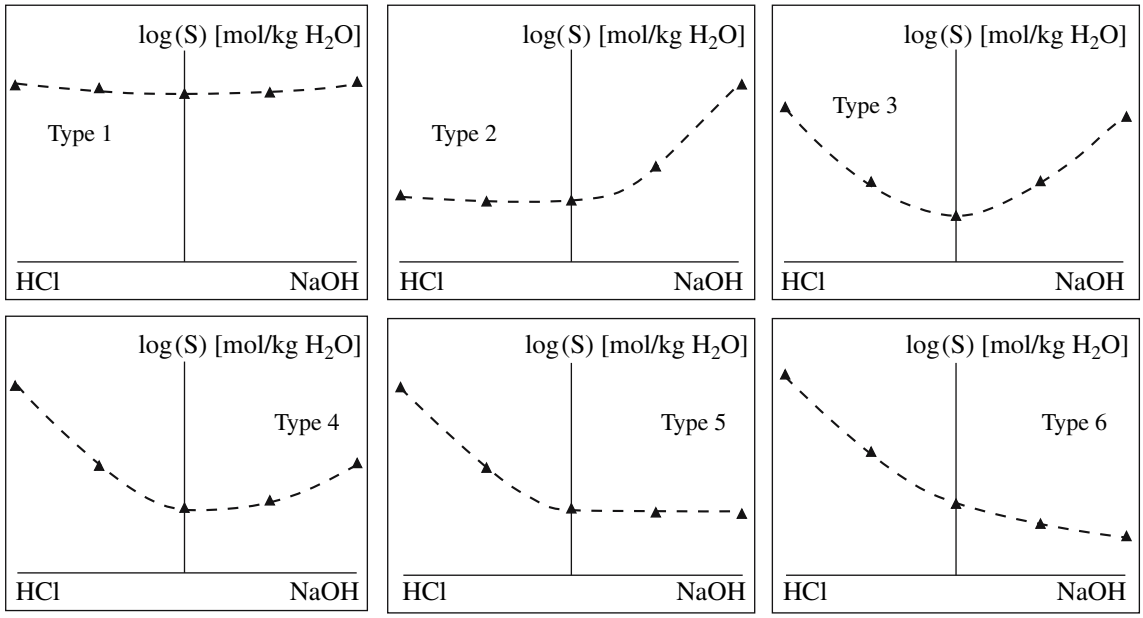

Fig. 11. Six types of solubility diagrams for minerals as functions of the acidity of metamorphic fluid. See text for a detailed discussion of these diagrams.

both in pure water and in slightly acidic solutions (Figs. 13–15). The solubility of micas and aluminum silicates increases significantly (by 2.0–3.5 orders of magnitude) in alkaline solutions and slightly increases in acidic solutions (0.1–1.0 M HCl). The solubility of corundum increases by 4.0–4.5 orders of magnitude in alkaline solutions. The solubility of corundum is almost constant in acidic fluids but increases by several orders (up to 3) of magnitude at low temperatures in strongly acidic fluids (0.1–1.0 M HCl). The minerals of this group (except for hematite) show an increase in solubility and its temperature dependence with increasing pressure. At low pressures (1 kbar), the solubility of these minerals (except for the solubility in strongly acidic solutions) is almost temperature-invariant, whereas at pressures of 3 and 5 kbar, the temperature effect becomes noticeable. Aluminum silicates and corundum show a change in the character of temperature dependence: it is positive for micas at any pressure, whereas for aluminous minerals of this group, it is nonmonotonous and passes through a maximum at 500°C and 1 kbar (Fig. 3) but is also positive at 3 and 5 kbar. At a given temperature, the solubility increases by approximately an order of magnitude as pressure increases from 1 to 5 kbar.

The behavior of hematite is strongly different from that of aluminous minerals. It shows the lowest solubility, and the shape of its diagram differs somewhat from those of other minerals of this group (Fig. 15). However, similar to other minerals of this group, the solubility of hematite increases dramatically (by 4–6 orders of magnitude) with increasing solution alkalinity and increases to a lesser extent in acidic solutions (especially at low temperatures). Another conspicuous feature of hematite solubility is its pronounced negative temperature dependence, which is observed at any pressure. At low pressure (1 kbar), the decrease of solubility with increasing temperature is especially significant in strongly acidic (up to 5 orders of magnitude) and strongly alkaline (2.0–2.5 orders of magnitude) solutions. At high pressures (5 kbar), the solubility is strongly affected by temperature only in acidic solutions (up to 6 orders of magnitude). In contrast, the temperature effect is negligible in alkaline solutions. At a given temperature, an increase in pressure from 1 to 5 kbar is accompanied by an increase in hematite solubility by 1.0–1.5 orders of magnitude in neutral solutions and by several orders of magnitude in acidic and alkaline solutions.

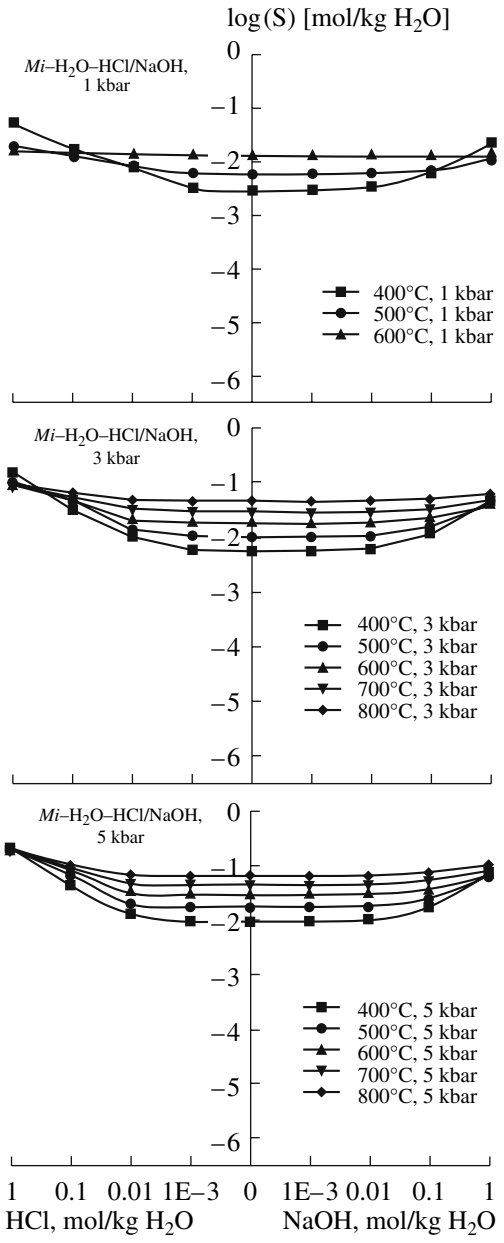

Fig. 12. First type of solubility diagrams. The dependence of microcline, $K(AlSi_3O_8)$, solubility on the acidity of fluid at pressures of 1, 3, and 5 kbar and temperatures of 400–800°C. The solubility is shown along the *y* axis in moles per one kilogram H_2O.

Type 3. The third type of solubility diagrams (Fig. 11) is observed in minerals enriched in amphoteric elements (Al and Fe): ferrous and magnesian staurolite, cordierite, chloritoid, almandine, spessartine, ferrous chlorite (chamosite), spinellids (spinel, hercynite, and magnetite), ferrous biotite (annite), sapphirines, and minerals consisting of FeO and SiO_2 (fayalite, ferrosilite, and grunerite). All of these minerals are in general less soluble than the minerals of the previous groups (except for hematite). They show the lowest solubility in pure water fluids (Figs. 17–19). Their solubility increases by 1.5–7.0 orders of magnitude in acidic solutions and by 1.0–4.5 orders of magnitude in alkaline solutions. The sequence of solubility for minerals of the third groups in neutral water fluid is shown in Fig. 20.

At a pressure of 1 kbar, the solubility of aluminous minerals (chloritoid, staurolite, spinel, sapphirine, cordierites, and almandine) decreases by 0.5–1.0 orders of magnitude with increasing temperature both in

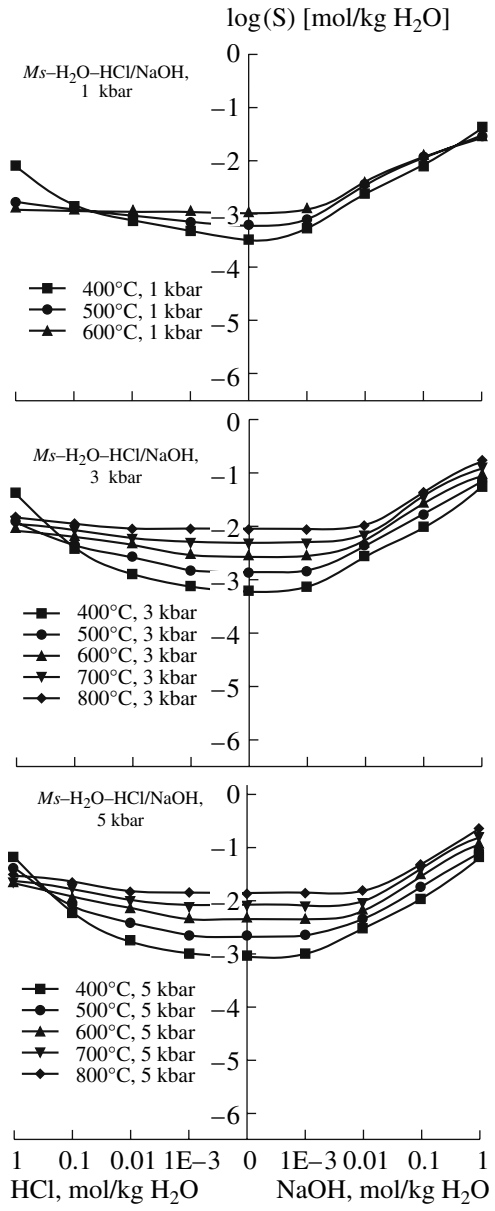

Fig. 13. Second type of solubility diagrams. The dependence of muscovite, $KAl_2(AlSi_3O_{10})(OH)_2$, solubility on the acidity of fluid at pressures of 1, 3, and 5 kbar and temperatures of 400–800°C. The solubility is shown along the *y* axis in moles per one kilogram H_2O.

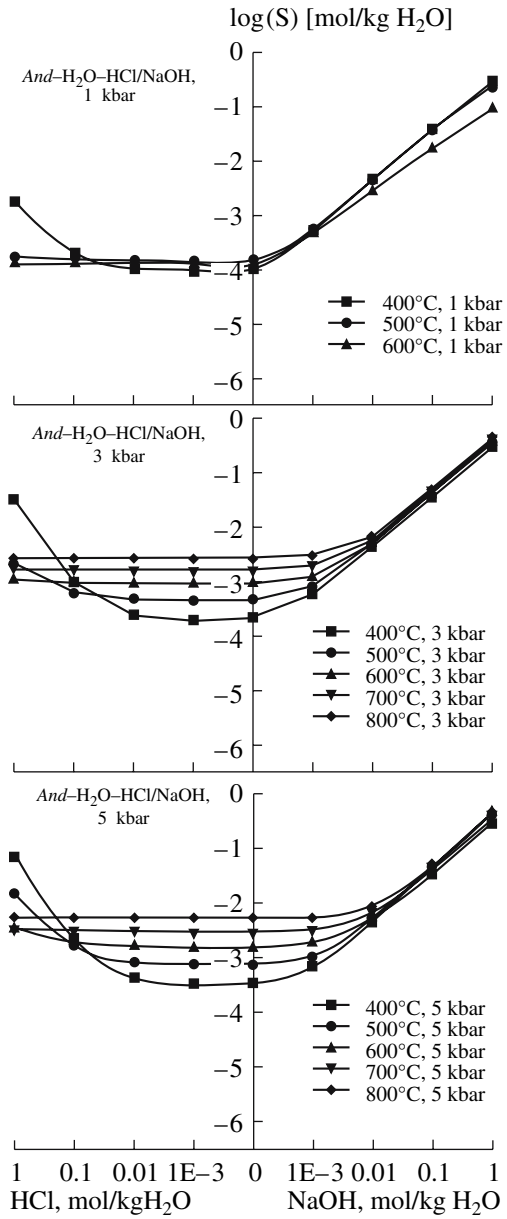

Fig. 14. Second type of solubility diagrams. The dependence of andalusite, Al_2SiO_5, solubility on the acidity of fluid at pressures of 1, 3, and 5 kbar and temperatures of 400–800°C. The solubility is shown along the *y* axis in moles per one kilogram H_2O.

acidic and alkaline solutions. For minerals with the highest iron contents (annite, chamosite, grunerite, ferrosilite, and fayalite), a slight temperature influence on solubility was observed only in alkaline solutions. The solubility of all group 3 minerals in water at low pressure show a weak temperature dependency of different character: nonmonotonous for staurolite, positive for ferrous minerals (chamosite, chloritoid, annite, ferrosilite, and grunerite), and complex (nonmonotonous) or negative for aluminous minerals (staurolites, sapphirines, spinels, and cordierites) and spessartine.

At 3 and 5 kbar, the maximum temperature effect on solubility was observed in neutral solutions, in a slightly acidic region for the most aluminous minerals, and in a slightly alkaline region for iron-rich minerals and spessartine. As pressure increases up to 3 and 5 kbar, most of the minerals of this group show a positive correlation between the solubility in neutral solutions and temperature, and the range of solubility variations increases compared with that observed at 1 kbar. In contrast, the temperature dependence of solubility becomes weaker in the acidic and alkaline regions.

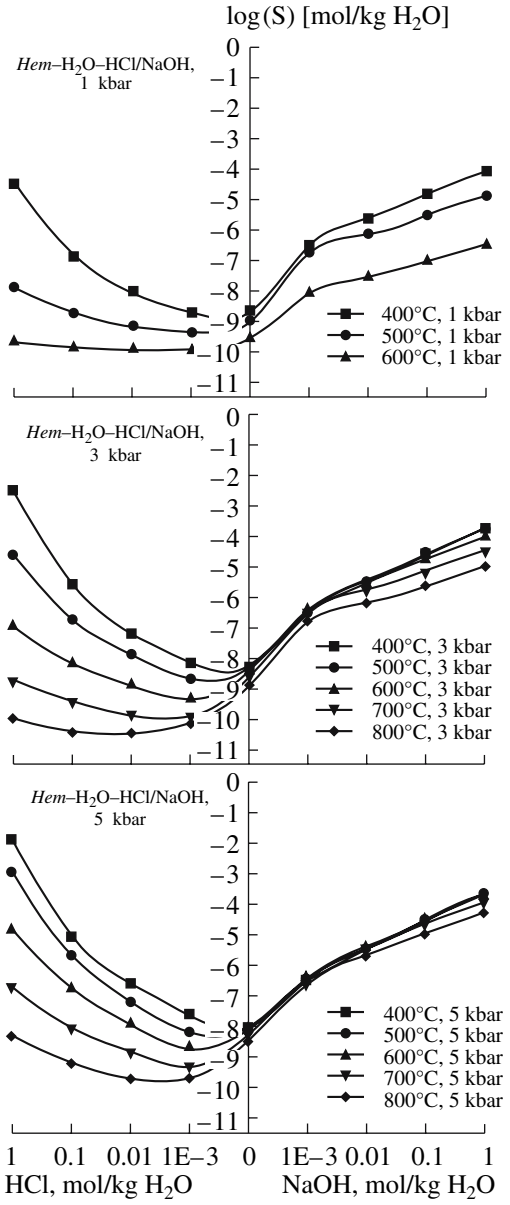

Fig. 15. Second type of solubility diagrams. The dependence of hematite, Fe_2O_3, solubility on the acidity of fluid at pressures of 1, 3, and 5 kbar and temperatures of 400–800°C. The solubility is shown along the *y* axis in moles per one kilogram H_2O.

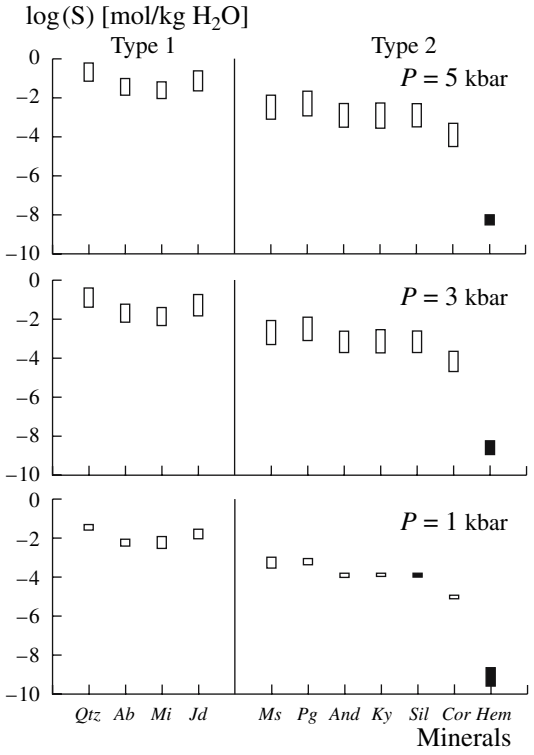

Fig. 16. Sequences of solubility of minerals with type 1 and 2 solubility diagrams under various pressures. The rectangles correspond to variations in solubility values within 400–600°C at 1 kbar and within 400–800°C at 3 and 5 kbar The solubility is shown along the *y* axis in moles per one kilogram H_2O. The shade of rectangles corresponds to the character of the temperature effect on solubility: open rectangles correspond to a positive correlation (solubility increases with increasing temperature); black rectangles correspond to a negative correlation; and gray rectangles correspond to nonmonotonous dependence (with a solubility maximum).

However, the temperature effect on the solubility of silica-poor aluminous minerals (sapphirines and spinellids) remains to be negative and decreases with increasing pressure. The absolute values of solubility of all the minerals also increase with increasing pressure.

Similar to hematite, magnetite is conspicuous among other minerals of this group, although its properties are more similar to those of other members of group 3. Similar to hematite, the temperature dependence of its solubility is negative at any pressure and is almost invariant with increasing pressure. Both in acidic and alkaline regions, it is much higher than that of other minerals of this group.

Type 4. The fourth type of solubility diagrams (Fig. 11) is characteristic of Al- or Fe-rich silicates of Ca and Mg: anorthite, lawsonite, epidote-group minerals (epidote and clinozoisite), magnesian chlorite (amesite), Ca–Fe amphibole (actinolite), and rhodonite. These minerals show the minimum solubility in pure water and weakly alkaline solutions (Figs. 21–22). Their solubility increases significantly (by 2.0–3.5 orders of magnitude) in acidic fluids and to a lesser extent (up to 1.0–1.5 orders of magnitude) in strongly alkaline fluids (0.1–1.0 M NaOH). At low pressures (1 kbar) the solubility of anorthite, epidote, and zoisite in neutral media slightly decreases with increasing temperature, and the solubility of lawsonite, amesite, actinolite, and rhodonite is independent of temperature (Fig. 24). With increasing pressure, the temperature coefficients of solubility become positive or nonmonotonous, and the range of solubility variations somewhat increases with temperature but remains moderate.

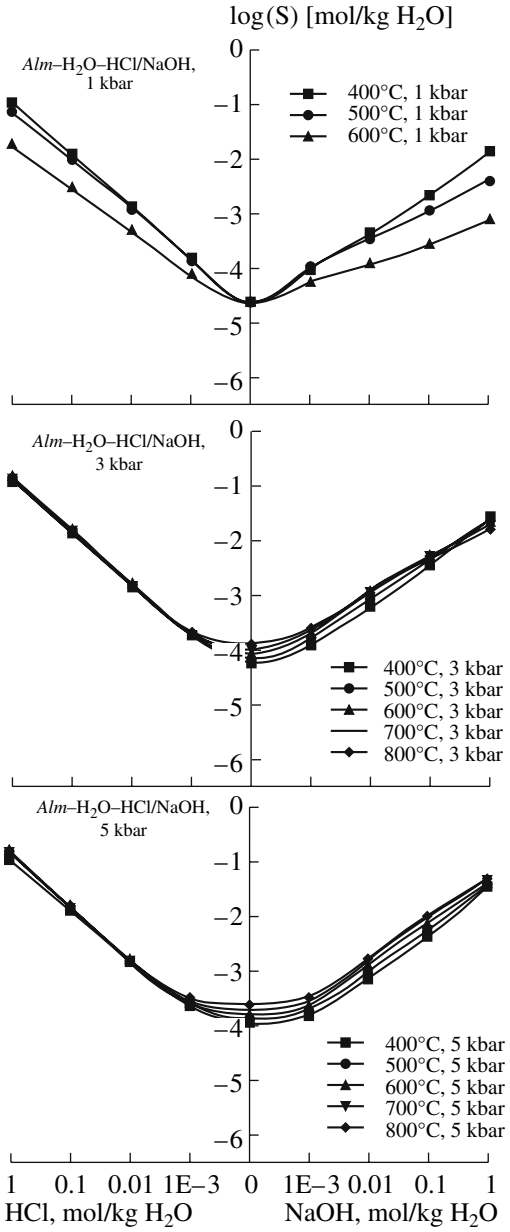

Fig. 17. Third type of solubility diagrams. The dependence of the solubility of almandine, $Fe_3Al_2(SiO_4)_3$, on the acidity of fluid at pressures of 1, 3, and 5 kbar and temperatures of 400–800°C. The solubility is shown along the *y* axis in moles per one kilogram H_2O.

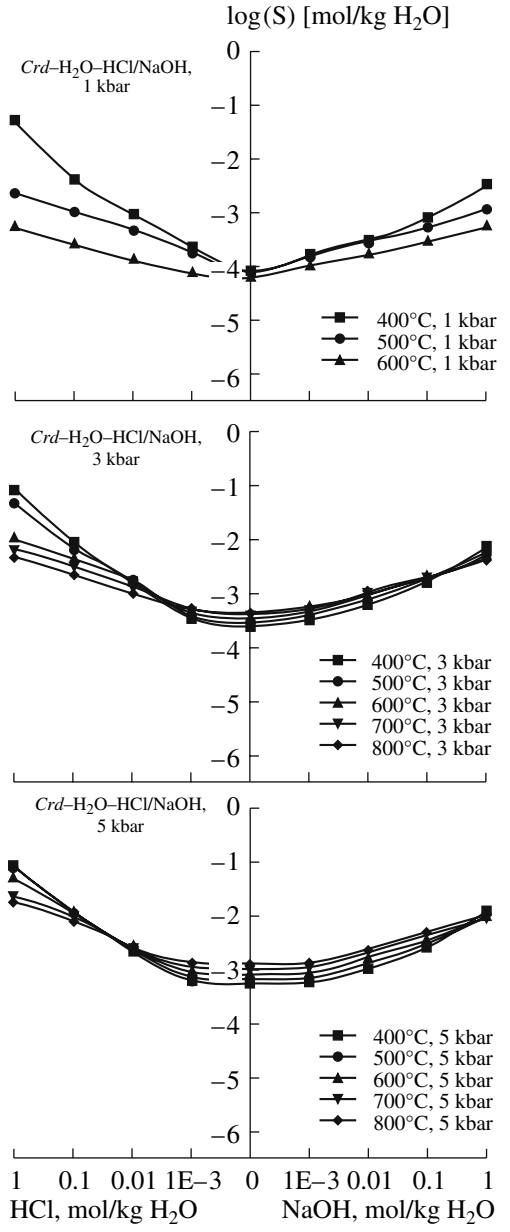

Fig. 18. Third type of solubility diagrams. The dependence of the solubility of cordierite, $Mg_2Al_3(AlSi_5O_{18})$, on the acidity of fluid at pressures of 1, 3, and 5 kbar and temperatures of 400–800°C. The solubility is shown along the *y* axis in moles per one kilogram H_2O.

The solubility of type 4 minerals in acidic and alkaline fluids is more sensitive to temperature than that in neutral fluids. The solubility of anorthite, amesite, epidote, zoisite, and lawsonite decreases in acidic media at 1 kbar by two orders of magnitude, whereas the solubility of actinolite and, to some extent, rhodonite remains almost constant. In alkaline fluids, temperature variations affect the solubility of actinolite, anorthite, epidote, zoisite (changes by one order of magnitude), and lawsonite (changes by 0.5 orders of magnitude), whereas the solubility of amesite is independent of temperatures. The solubility of rhodonite in weakly alkaline fluids is independent of temperature, but in strongly alkaline fluids it decreases dramatically with increasing temperature, and the higher the solubility increase with increasing alkalinity is, the greater is the temperature effect. The solubility of actinolite, zoisite, lawsonite, and rhodonite at 3 and 5 kbar is also temperature-independent in acidic solutions, whereas the solubility varies by 0.5 orders of magnitude (0.75 for law-

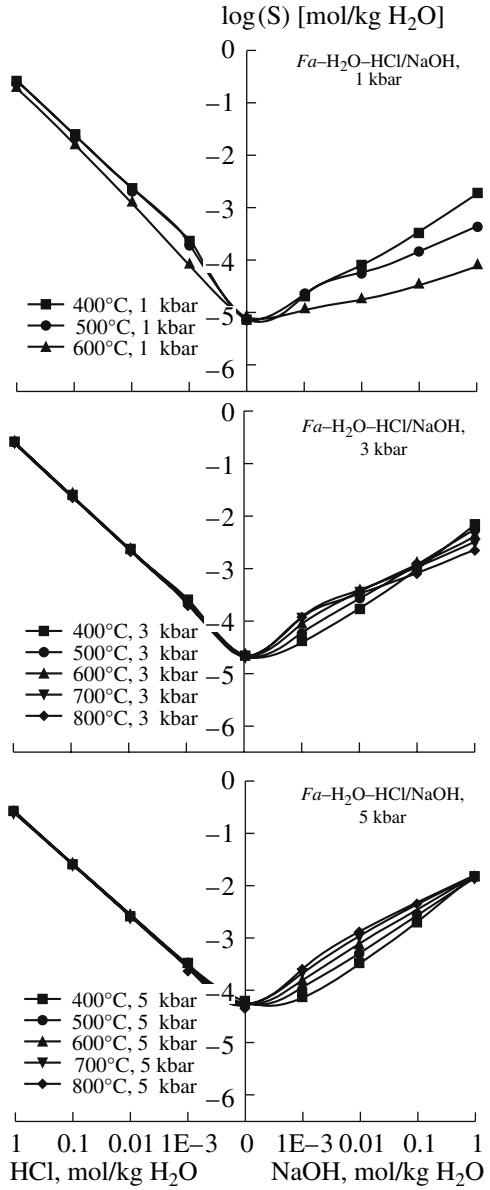

Fig. 19. Third type of solubility diagrams. The dependence of the solubility of fayalite, $Fe_2(SiO_4)$, on the acidity of fluid at pressures of 1, 3, and 5 kbar and temperatures of 400–800°C. The solubility is shown along the *y* axis in moles per one kilogram H_2O.

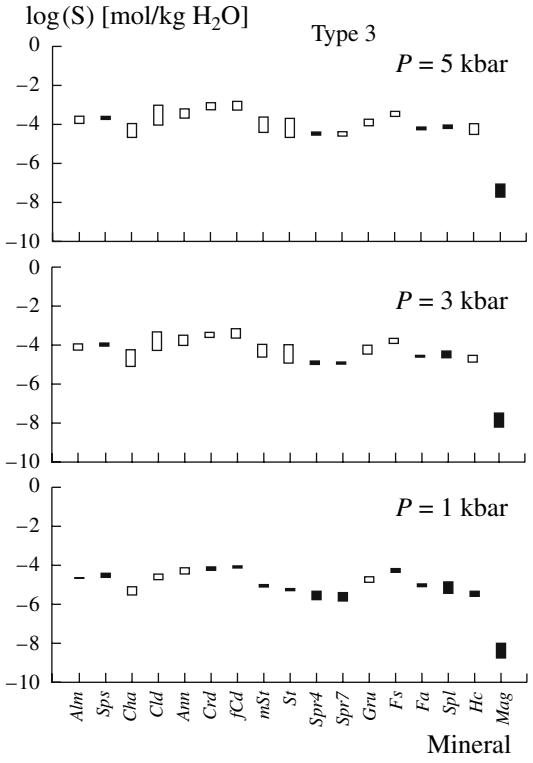

Fig. 20. Sequences of solubility for minerals with type 3 solubility diagrams at various pressures. Symbols are the same as in Fig. 16.

sonite) in weakly alkaline fluids. The solubility of anorthite, amesite, and epidote in acidic fluids decreases with increasing temperature by more than an order of magnitude at 3 kbar, but this dependence weakens at 5 kbar. The solubility of anorthite and zoisite decreases slightly with increasing temperature in alkaline fluids, whereas that of amesite increases. The solubility of all the minerals increases to a varying degree with increasing pressure.

Type 5. The fifth type of solubility diagrams (Fig. 11) is characteristic of Al- and Fe-bearing silicates with high contents of Ca and Mg: garnets (pyrope, grossular, and andradite), calcic clinopyroxene (hedenbergite), some amphiboles (tschermakite, gedrite, and riebeckite), vesuvianite, prehnite, and magnesian chlorite (clinochlore). These minerals show the minimum solubility in pure water and alkaline solutions (Fig. 23). Their solubility in acid media is 2–4 orders of magnitude higher than that in water. The solubility sequence of type 5 minerals in pure water fluids is shown in Fig. 24. At low pressure, the solubility of all the minerals of this group is inversely dependent on temperature (except for riebeckite, the solubility of which is temperature invariant), and varies within 0.2–0.5 orders of magnitude. As pressure increases up to 3 kbar, the temperature effect on the solubility becomes nonmonotonous for most of the minerals, positive for riebeckite, and negative for pyrope and andradite. Correspondingly, the range of solubility variations decreases for all the minerals except for riebeckite. This range increases up to 0.45 in the case of riebeckite. At 5 kbar, the correlation of temperature with solubility is positive for most of the minerals (although the extent of solubility variations is only 0.2–0.3 order of magnitude), negligible for grossular, pyrope, and vesuvianite, and negative for andradite (its solubility decreases between 400 and 800°C by 0.3 order of magnitude).

At low pressures (1 kbar), the solubility decreases with increasing temperature by 1.5–2.0 orders of magnitude (0.35 for riebeckite) in acidic solutions and by

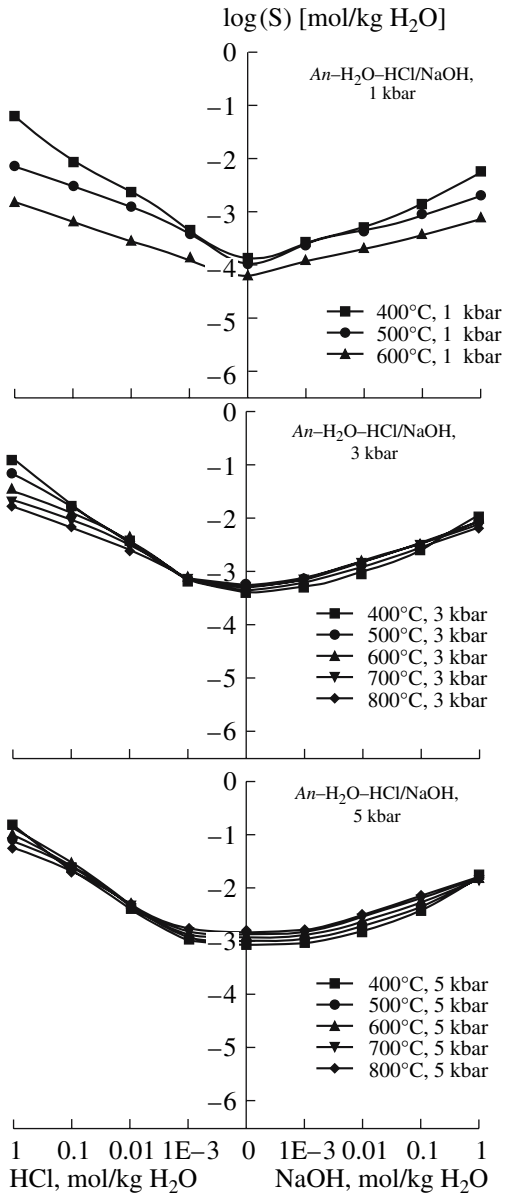

Fig. 21. Fourth type of solubility diagrams. The dependence of the solubility of anorthite, $Ca(Al_2Si_2O_8)$, on the acidity of fluid at pressures of 1, 3, and 5 kbar and temperatures of 400–800°C. The solubility is shown along the *y* axis in moles per one kilogram H_2O.

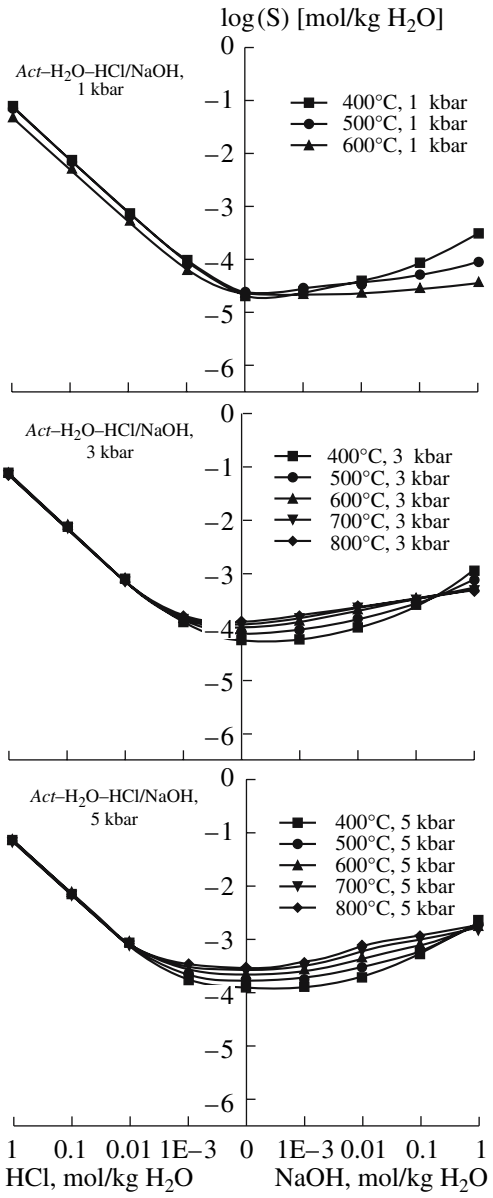

Fig. 22. Fourth type of solubility diagrams. The dependence of the solubility of actinolite, $Ca_2Fe_5(Si_8O_{22})(OH)_2$, on the acidity of fluid at pressures of 1, 3, and 5 kbar and temperatures of 400–800°C. The solubility is shown along the *y* axis in moles per one kilogram H_2O.

0.5–1.0 order of magnitude in alkaline solutions. The temperature dependence of solubility in acidic solutions practically vanishes with increasing pressure. An exception is andradite, the solubility of which in acidic solutions at 5 kbar decreases by an order of magnitude as temperature increases from 400 to 800°. The solubility of the majority of minerals of this group in alkaline fluids is weakly dependent on temperature at 5 kbar, varying by no more than 0.25 order of magnitude. The solubility of andradite in both alkaline and acidic fluids decreases with increasing temperature by an order of magnitude, whereas the solubility of clinochlore, prehnite, and riebeckite increases slightly (approximately by 0.5 order of magnitude).

Type 6. The diagrams of this type (Fig. 11) were obtained for the solubility of oxides and hydroxides of Mg and Ca (periclase, brucite, and portlandite), silicates of Mg and Ca, including Mg and Ca–Mg amphiboles (anthophyllite, cummingtonite, and tremolite), pyroxenes (enstatite and diopside), olivine (forsterite),

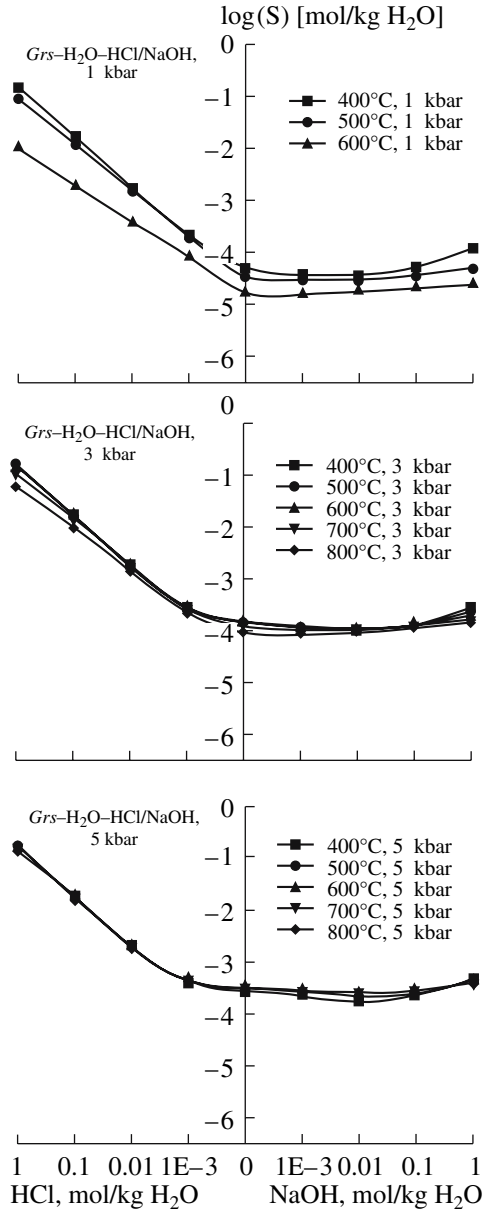

Fig. 23. Fifth type of solubility diagrams. The dependence of the solubility of grossular, $Ca_2Al_3(SiO_4)_3$, on the acidity of fluid at pressures of 1, 3, and 5 kbar and temperatures of 400–800°C. The solubility is shown along the *y* axis in moles per one kilogram H_2O.

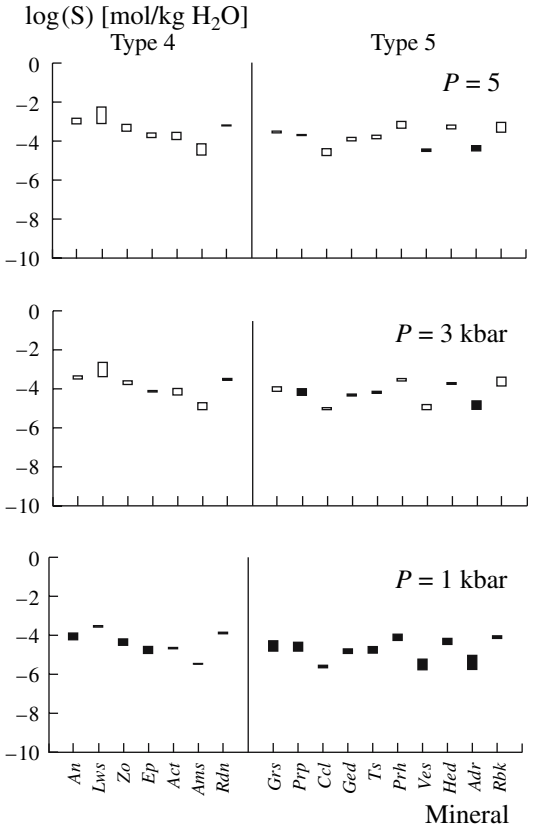

Fig. 24. Sequences of solubility for minerals with type 4 and 5 solubility diagrams at various pressures. Symbols are the same as in Fig. 16.

magnesian biotite (phlogopite), wollastonite, clinohumite, talc, serpentine (chrysotile), Na-bearing magnesian amphiboles (pargasite and glaucophane), and alkaline pyroxene (aegirine). These minerals show the minimum solubility in strongly alkaline solutions (Figs. 25, 26). Compared with neural fluids, the solubility of these minerals increases significantly in acidic solutions (by 2.5–4.5 orders of magnitude) and decreases in alkaline solutions (by 1–3 orders of magnitude).

The sequence of solubility of these minerals in a neutral water fluid is shown in Fig. 27. At low pressures (1 kbar), the solubility of most of the minerals changes insignificantly or slightly declines (by 0.2–0.7 order of magnitude) with increasing temperature. The greatest changes in solubility were obtained for portlandite (by 1.3 orders of magnitude) and periclase (by 1.1 orders of magnitude). The solubilities of all the minerals of this group, except for glaucophane, are negatively correlated with temperature. At 3 kbar, the negative temperature effect on the solubility is retained for most of these minerals, but it becomes nonmonotonous (and very weak) for alkali-bearing minerals (aegirine, pargasite, and phlogopite), tremolite, and talc. The solubility of glaucophane is positively correlated with temperature both at low and high pressures. At 5 kbar, the temperature dependence of solubility is positive for glaucophane and aegirine, almost negligible for the majority of minerals, and negative for periclase, brucite, portlandite, wollastonite, forsterite, enstatite, and clinohumite.

An increase in temperature at 1 kbar has almost no influence on the solubility of brucite, periclase, and portlandite. The solubility of alkali-free Ca and Mg silicates decreases by 0.5–1.5 orders of magnitude and that of alkali-bearing silicates decreases by 1–2 orders of magnitude with increasing temperature. The solubil-

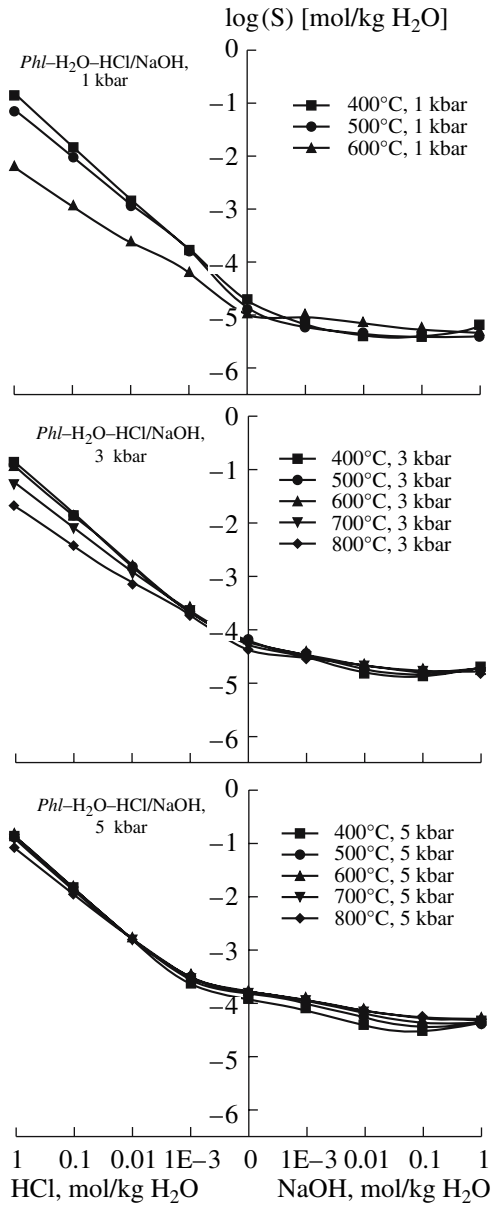

Fig. 25. Sixth type of solubility diagrams. The dependence of the solubility of phlogopite, $KMg_3(AlSi_3O_{10})(OH)_2$, on the acidity of fluid at pressures of 1, 3, and 5 kbar and temperatures of 400–800°C. The solubility is shown along the *y* axis in moles per one kilogram H_2O.

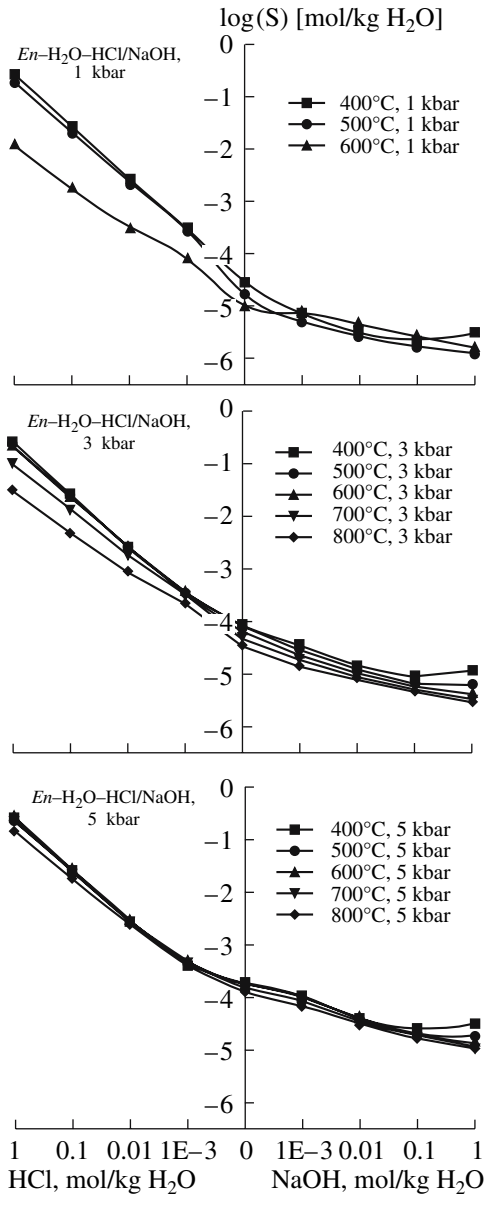

Fig. 26. Sixth type of solubility diagrams. The dependence of the solubility of enstatite, $Mg_2(Si_2O_6)$, on the acidity of fluid at pressures of 1, 3, and 5 kbar and temperatures of 400–800°C. The solubility is shown along the *y* axis in moles per one kilogram H_2O.

ity of minerals in an alkaline medium at 1 kbar does not change or slightly decreases. At high pressures (3 and 5 kbar), the solubility of minerals in acidic solutions does not change or decreases slightly (up to 0.5 order of magnitude, but up to 1 order of magnitude for aegirine). The solubility of alkali silicates in alkaline solutions under these pressures is practically invariant, that of Ca and Mg silicates decreases by up to 0.6–0.7 order of magnitude, and that of periclase and portlandite decreases by 1.6–1.7 orders of magnitude.

4.3. Influence of Acidity–Alkalinity on the Solubility of Minerals

As can be seen from the diagrams, the solubility of almost all minerals is primarily controlled by the acidity–alkalinity of the fluid, whereas the effect of *P–T* conditions is smaller. The only exception is the solubility of first-type minerals, for which the influence of temperature and pressure is comparable or even higher than that of fluid acidity.

4.4. Influence of Temperature and Pressure

Temperature. In neutral solutions, the effect of temperature is more significant (by about one order of magnitude or more) for the minerals of types 1–3. The solubility of all minerals of the first type and some minerals of the second type increases with increasing temperature and pressure. With increasing temperature, the solubility of type 2–5 minerals and alkali-bearing minerals of type 6 weakly changes or decreases at low pressures and increases at high pressures (5 kbar). The solubility of other (alkali-free) minerals of type 6 decreases or weakly changes with increasing temperature even at 5 kbar. Exceptions for various types are hematite, magnetite, and andradite, the solubility of which decreases with increasing temperature at any pressure. Thus, with increasing pressure, the temperature dependence of solubility may remain unchanged or transform from negative to positive but not vice versa. On the other hand, with increasing temperature, the temperature effect may persist or change from positive to negative (nonmonotonous character of temperature dependence with a solubility maximum). Minima were never observed on the solubility–temperature curves. In acidic or alkaline solutions, the dependence of solubility on temperature is even more complex.

Pressure. An increase in solubility with increasing pressure was previously established for subcritical or near-critical (~0.25–0.50 kbar) pressures [58, 59]. Our results extend this conclusion to higher pressures. Such behavior is obviously related to the increasing density and dielectric constant of fluid, which enhances its dissolving capacity. The solubility of all of the minerals in neutral solutions increases by 1–2 orders of magnitude as pressure increases from 1 to 5 kbar. The role of pressure becomes more significant with increasing temperature. In acidic or alkaline solutions, the solubility also increases with increasing pressure, but this dependence becomes more complex. The solubility of type 1 minerals increases by approximately 0.5 order of magnitude in acidic and alkaline fluids. For the minerals of the second type, the pressure effect on the solubility is more pronounced in acidic solutions (an increase by 0.3–2.0 orders of magnitude) than in alkaline solutions (an increase by 0.2–0.5 orders of magnitude). An exception is hematite, the solubility of which may increase by 4 orders of magnitude in acidic solutions and 3 orders of magnitude in alkaline media. The higher the temperature, the stronger the pressure effect in acidic fluids. The solubility of the majority of minerals of other types increases both in acidic and alkaline solutions by approximately 0.3–2.0 orders of magnitude.

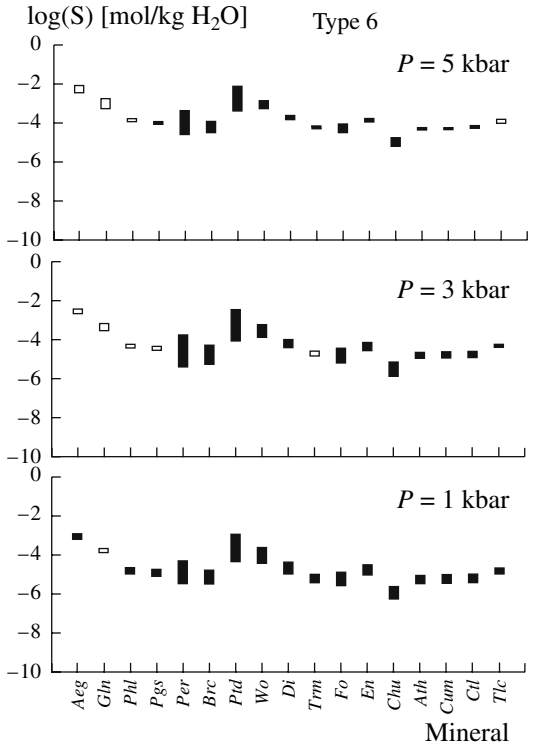

Fig. 27. Sequences of solubility for type 6 minerals in aqueous fluids at pressures of 1, 3, and 5 kbar and temperatures of 400–800°C. Symbols are the same as in Fig. 16.

5. DISCUSSION

5.1. Mobility of Elements in Aqueous Fluids

The dependence of the solubility of minerals on their compositions and the analysis of mineral behavior in fluids of various compositions allow us to characterize the mobility of elements composing the minerals as a function of fluid acidity. Such an approach is based on a simultaneous comparison of the compositions of minerals, their solubilities, and the topology of solubility diagrams. For instance, the solubility of minerals in the $MgO–SiO_2–H_2O$ system decreases with increasing Mg/Si value (Fig. 28) up to the minimum solubility of brucite; this is accompanied by an increase in the extent of fluid acidity effect on the solubility. The decrease of solubility with increasing Mg/Si implies Si mobility and inert behavior of Mg in a neutral medium. The increase of solubility in an acidic environment is more pronounced for minerals with higher Mg contents, which indicates that Mg is responsible for the solubility increase in acids. The decrease of solubility in alkaline solutions is also related to the inert behavior of Mg in alkaline environments. The influence of Mg on the behavior of minerals in this system is so pronounced that all of these minerals were assigned to group 6 with respect to the character of solubility. The type of solubility diagrams in more complex systems is controlled by the proportions of components. For instance, the diagrams of minerals of the $MgO–Al_2O_3–SiO_2–H_2O$ system belong, depending on the Mg/Al ratio, to the third (Mg-staurolite, cordierite, sapphirines, and spinel), fourth (amesite), and fifth (pyrope, clinochlore, and gedrite) topological types (Fig. 29a). For minerals with identical Mg/Al ratios, the topologies of diagrams

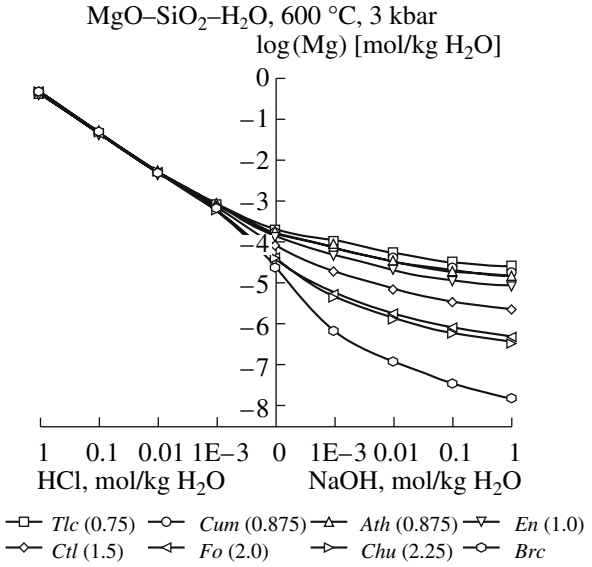

Fig. 28. Character of the solubility of minerals in the $MgO–SiO_2–H_2O$ system. The numbers near mineral symbols indicate the Mg/Si ratio.

are similar, and the solubility is controlled by the amount of Si in the minerals (Fig. 29b).

A comparison of the behavior of minerals of different compositions belonging to different groups (feldspars, micas, chlorites, amphiboles, pyroxenes, garnets, etc.) suggests that the solubility of minerals is almost independent of their structure and is controlled almost entirely by composition. For instance, the third group includes all of the minerals of the $FeO–Al_2O_3–SiO_2–H_2O$ system, among which are orthosilicates (almandine, staurolite, and chloritoid), a cyclosilicate (Fe-cordierite), and chlorite (chamosite). A similar behavior was observed for ferrous biotite (annite), which is chemically similar to them. The minerals of the $MgO–SiO_2–H_2O$ system belonging to the sixth group include orthosilicates (forsterite and clinohumite), pyroxene (enstatite), amphiboles (anthophyllite and cummingtonite), and phyllosilicates (chrysotile and talc).

The analysis of diagrams presented in this paper shows that quartz and alkali aluminosilicates are the most soluble minerals, and the solubility decreases with decreasing contents of alkalis and silica and increasing content of aluminum (cf. feldspars and micas). The solubility of alkali-free aluminum silicates is significantly lower, and pure alumina (corundum) is even less soluble. This means that the mobility of silica is weakly dependent on the acidity of fluid (or even completely independent in acidic solutions) and is mainly controlled by *P–T* conditions. The concentration of silica in solution may be as high as 0.7 mol/kg H_2O (in equilibrium with quartz at 800°C and 5 kbar). The mobility of alkalis in solutions is high at any acidity and is much more sensitive to *P–T* conditions. The concentrations of alkalis in equilibrium solution may be up to 0.05–0.10 mol/kg H_2O.

Calcium, magnesium, iron (II), and manganese (II) are mobile in acidic solutions. Their mobility increases significantly with increasing acidity. The concentrations of Fe(II) and Mg in acidic solutions in equilibrium with minerals may be up to 0.1–0.3 mol/kg H_2O, and that of Ca is up to 0.5 mol/kg H_2O. Iron (II) and manganese (II) are mobile in strongly alkaline solutions, albeit to a lesser extent than in acidic solutions (up to 0.3 mol Fe^{+2}/kg H_2O), whereas the mobilities of Mg and Ca are rather low (less that 3×10^{-4} and 2×10^{-5} mol/kg H_2O, respectively).

The least mobile components are aluminum and ferric iron. Their low mobility is indicated by the solubility of corundum and hematite. The content of Al in a fluid in equilibrium with corundum ranges from the lowest value of 1.5×10^{-5} mol/kg H_2O (400°C, 1 kbar, and 10^{-3} M HCl solution) to 0.9 mol/kg H_2O (800°C, 5 kbar, and 1 M NaOH solution). The mobility of Al increases markedly with increasing alkalinity. The equilibrium concentrations of Fe(III) in solutions are much lower than those of Al (Fig. 16): they are no higher than 10^{-8} mol/kg H_2O in neutral solutions and reach 10^{-3}–10^{-2} mol/kg H_2O in strongly acidic solutions at 5 kbar. Given the estimates of hematite and magnetite solubility, it can be supposed that Fe must be transported in solutions mainly as ferrous species, and its oxidation must occur immediately during the crystallization of minerals containing Fe(III). This inference is supported by a comparison with experimental data showing that the solubility of magnetite and hematite is very low in an oxidizing environment, where ferric iron is stable in solution, and only ferrous iron occurs in solutions under more reducing conditions [60, 61].

Thus, alkalis (Na and K) and divalent bases (primarily, Ca and Mg, followed by Fe^{+2} and Mn^{+2}) are the most mobile components during *acid leaching*. Ferric iron is mobile in strongly acidic solutions. Aluminum is less mobile (except for ultra-acidic solutions). The behavior of Si depends on the composition of solution. It will not be dissolved in the solutions that were preliminarily saturated in silica (for instance, acidic solutions released from a granite magma or generated by decompression in metamorphic complexes). However, owing to changes in solubility at the expense of temperature or pressure variations, these solutions will deposit quartz in the form of, say, quartz veins of silicified zones. Quartz will be mobile in the acidic solutions that were not initially saturated in SiO_2 (for instance, solutions related to basic volcanism). Na and K are also mobile in alkaline solutions. They are joined by Al and Si and, to a lesser extent, by Fe^{2+} and Mn^{2+}. Mg and Ca must be inert in alkaline solutions, and their mobility decreases with increasing alkalinity. In *neutral aqueous solutions*, N, K, and Si are mobile, while the bases (Ca, Mg, Fe^{2+}, and Mn^{2+}) and Al are inert. Correspondingly,

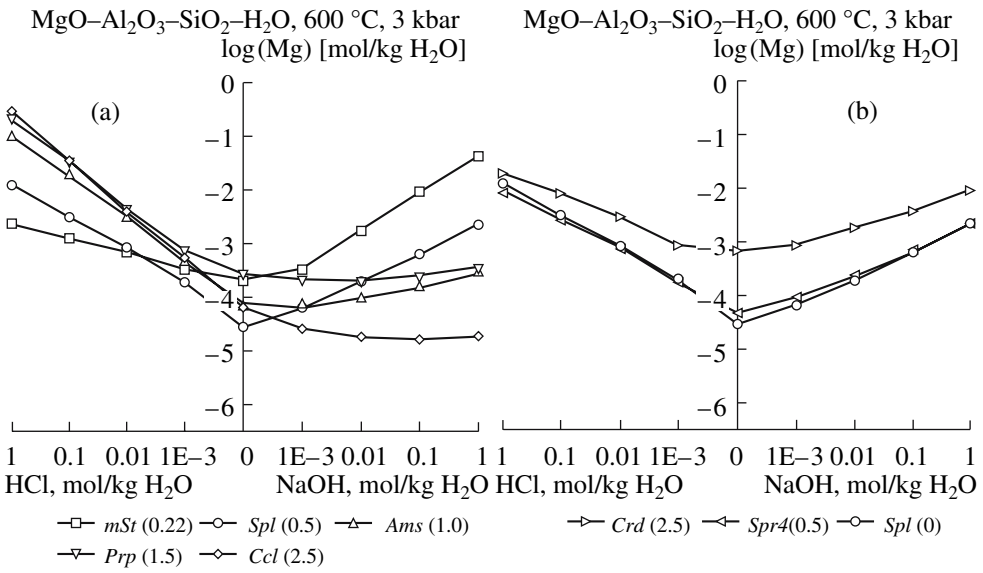

Fig. 29. Character of the solubility of minerals of the $MgO–Al_2O_3–SiO_2–H_2O$ system (a) for different Mg/Al ratios and (b) for different Mg/Si ratios (at constant Mg/Al). The numbers near mineral symbols indicate the ratios of (a) Mg/Al and (b) Si/Mg.

changes in acidity must result in the dissolution of some components and deposition of others.

It is instructive to compare these inferences with direct experimental observations of element mobility, in particular, with the results reported by Zaraiskii [62, 63]. Summarizing a series of experiments, he proposed the following sequence of element mobility during the acid leaching (under the influence of HCl) of felsic rocks (granites and quartz diorites):

K, Na | Ca, Mg, Fe | Si, Al, Ti.

It is readily seen that this sequence is similar to that obtained by us for acidic fluids.

For alkaline solutions (sodic metasomatism), Zaraiskii reported a different mobility sequence:

Na | Ca, Si, K, Al | Mg, Fe, Ti.

This sequence differs somewhat from that obtained here, and is therefore considered in more detail. The mobility sequences were determined by Zaraiskii on the basis of the occurrence of phases incorporating the respective elements in the zones of the column. In addition, he also established the sequences of migration activity [63, p. 131], which were quantitatively characterized by changes in concentrations in the column owing to element input or output. The sequences of mobility and migration activity deduced by Zaraiskii are identical for acid leaching. For alkaline metasomatism, Zaraiskii reported the following sequences of migration activity:

K > Si > Al > Mg > Fe > Ca > Ti (column 3: granite + Na_2CO_3 + NaCl, 500°C);

Si > Al > K > Ca > Mg > Fe > Ti (column 4: Bt schist + Na_2CO_3 + NaCl, 500°C).

Potassium was considered as a moderately mobile component on the basis of potassium feldspar stability in the intermediate zones of the column; however, potassium appeared to be mobile in the above sequences. In contrast, calcium was classified by Zaraiskii as a mobile component, because it does not from its own phases. However, the initial rocks (granite and mica schist) affected by metasomatism were also free of calcium phases. Therefore, it is difficult to assess the mobility of this element. In the sequence of migration activity, calcium is a low-mobility (inert) component. The inert behavior of iron is evidently related to its occurrence in the system as ferric iron in the composition of alkali pyroxenes and amphiboles. As was shown above, these minerals are poorly soluble in alkaline fluids and define, therefore, the inert behavior of Fe(III). Unfortunately, Zaraiskii did not report data on the mobility of Fe(II) in an alkaline environment. Thus, the tendencies of element mobility in alkaline fluids observed in the experiments of Zaraiskii and expressed as the sequences of migration activity are in good agreement with our conclusions, including the high mobility of silicon and alkalis, mobility of aluminum, and low mobility of bases. Thus, it is more plausible to estimate mobility sequences on the basis of the extent of element gain and loss rather than from the phase compositions of metasomatic zones.

A considerable increase in the solubility of Fe–Mg minerals and in the mobility of bases (Mg and Fe) in acidic solutions compared with neutral ones was experimentally established by Purtov et al. [64–66]. These authors also noticed that the solubility of iron compounds increases in alkaline environments, although to a lesser extent than in acidic solutions. Magnesium behaves as an inert component in an alkaline environment. In contrast to acidic fluids, the mobility of these elements in pure water is low [67]. Purtov et al. also

established low aluminum mobility in neutral solutions. Thus, the experimental investigations of element mobility support our conclusions. These observations allow us to consider the solubility of minerals in aqueous fluids as one of the main indicators of element mobility during metasomatism. In particular, the consistency of our conclusions with the experimental results of Zaraiskii, which was discussed above, clearly shows that, although these experiments reproduced diffusion metasomatism, the mobility of elements was controlled by the values of solubility rather than by diffusion rates, which are similar for the majority of elements and only slightly sensitive to the acidity of the system [68, 69].

5.2. Analysis of Metasomatic Columns and Behavior of Minerals during Metasomatism

Minerals from different groups respond differently to variations in solution acidity, and they may therefore be good indicators for the acidity–alkalinity conditions of metasomatizing solutions. In the simplest cases, it is sufficient to analyze the minerals of the inner zones of the column approaching equilibrium with the metasomatizing solution. For instance, the accumulation or appearance of low-solubility minerals of the second type in the inner zones of a metasomatic column indicates that it was formed under the influence of acidic solutions (acid metasomatism or acid leaching). If minerals of the fifth or sixth type are accumulated or appear, the column was formed under the influence of alkaline or neutral solutions (alkaline or basic metasomatism). In more complicated and ambiguous cases, it may be necessary to analyze the behavior of minerals in the inner, medium, and outer zones of the column.

During acid metasomatism, changes in mineral composition toward inner zones must be controlled by differences in the migration mobility of major elements composing the minerals. In particular, with increasing acidity, the accumulation of least mobile (most inert) elements in the inner zones of acid columns can stabilize Fe–Mg minerals enriched in Al and Fe^{3+} (e.g., cordierite, staurolite, garnet, and magnetite), and minerals with high Si and Al contents must be accumulated. Such a process may produce metasomatic cordierite–andalusite and staurolite–andalusite quartzites [70–72]. A further increase in acidity results in the dissolution of Fe–Mg minerals and continuing accumulation of aluminous minerals, for instance, andalusite, in the inner zone.

Since K and Na can be highly mobile in solutions of any acidity, albite–andalusite and muscovite–andalusite quartzites may be formed in the proximal zones of acid columns, and quartz–albite rocks and albitites develop in the proximal zones of alkalic columns. The solubility of white micas increases relative to that of aluminum silicates with increasing solution acidity; therefore, the disappearance of micas coupled with the accumulation of kyanite, andalusite, or sillimanite together with quartz can be expected in the proximal zones of columns of acid leaching. In neutral solutions at low pressures, sodic plagioclases are less stable than calcic ones. The stability of sodic plagioclases in sodium-rich solutions probably increases with increasing acidity, and their accumulation in proximal zones can be expected.

The detailed analysis of natural metasomatic complexes on the basis of relations derived in this study will be the subject of future investigations.

5.3. Chemical Signature of Solutions

The investigation of the composition of solution in equilibrium with metamorphic rocks is one of the most efficient ways for the determination of the composition of metamorphic fluids [2, 4]. Therefore, the obtained results and relations derived on the basis of these data provide insight into the compositions of solutions participating in metamorphic reactions. Since quartz and feldspars show the highest solubility and occur in most metamorphic rocks, the metamorphic fluids must be usually saturated in silica. In addition, significant amounts of alkalis must be transported into solutions owing to feldspar dissolution. When minerals of other types are decomposed, silica and alkalis are dominant components in neutral and acidic aqueous solutions. These solutions may become oversaturated in these components at a decrease in temperature and pressure (for instance, during cooling or exhumation of massifs). This produces aggressive silica–alkali fluids [73], which cause large-scale Na–Si and K–Si metasomatism and granitization, both areal and confined to the zone of high permeability [74–76].

The solubility of Fe- and, especially, Mg- and Ca-bearing minerals in alkaline solutions is low compared with acidic solutions. Therefore, acid leaching must be the main mechanism of the formation of base-rich solutions. The interaction of primary acidic solutions, either metamorphic or released from a magma, with mafic and ultramafic rocks results in the leaching of bases and accumulation of silica and aluminum with the formation of secondary quartzites with kyanite, andalusite, muscovite, and other aluminous phases [77]. Correspondingly, the solutions are enriched in Mg, Ca, and Fe and can deposit these elements in response to a decrease in temperature and pressure or owing to a reaction with contrasting rocks (e.g., during skarn formation in granites or gneisses, basic iron–magnesium metasomatism, and other similar processes) [78]. Such a process can be referred to as basification [79].

Since the mobility of ferric iron is also strongly dependent on acidity (decreases dramatically with decreasing acidity, Fig. 15), the neutralization of initially acidic postmagmatic fluid during the formation of skarns may lead to the deposition of considerable amounts of magnetite, which is observed, for example,

in the skarns of Pitkäranta [80], western Carpathians [81], Aldan [82], and many other regions.

In contrast to Mg- and Ca-rich solutions, fluids enriched mainly in Fe could initially be both acidic and alkaline. Such fluids may be responsible for alkaline metasomatism in iron formations resulting in their enrichment in iron [83, 84].

The chemistry of aqueous fluid controls also the composition of solid solutions crystallizing from it and, consequently, the character of zoning in the crystals. It was shown by us previously [85] that the acidity of fluid exerts a major influence on the partition of elements between growing metamorphic garnets and their parental fluid.

Finally, it should be noted that the calculated solubility values reported here will be refined, as the models and thermodynamic properties of minerals and aqueous species are improved; however, we hope that the main tendencies considered in this paper will be retained.

CONCLUSIONS

(1) In general, recent models and available thermodynamic data adequately describe the experimental measurements of mineral solubility in supercritical fluids.

(2) The solubility diagrams of oxide and silicate minerals of metamorphic and metasomatic rocks can be divided into six types with respect to the character of mineral solubility in pure water, acids, and alkalis. The minerals belonging to a particular type show common features in the behavior during interaction with aqueous fluids.

(3) The solubility of minerals of all types (except for the first type) is primarily controlled by the acidity–alkalinity of fluid (pH) and, to a lesser extent, by *P–T* conditions. The solubility of minerals of the first type (quartz, jadeite, and alkali feldspars) is controlled by variations in *P–T* conditions and is weakly dependent on the acidity of solutions.

(4) Minerals from various groups can be used as indicators of the acidity–alkalinity of parental solutions during the investigation of metasomatic processes. The analysis of solubility diagrams for minerals from various zones of a metasomatic column provides a means for estimating the chemical composition and acidity properties of solution and evaluating the influence of the composition of these solutions on changes in the mineral composition of metasomatic rocks.

(5) The dependence of the solubility of minerals on their compositions and a comparison of mineral behavior in fluids of various compositions allowed us to characterize the mobility of elements composing these minerals as a function of fluid acidity and estimate their concentrations in solutions.

(6) Since quartz shows the highest solubility and occurs in the majority of metamorphic rocks, metamorphic fluids must be usually saturated in silica. The appearance of aggressive silica–alkali fluids promoting metasomatic alterations in metamorphic complexes can be explained by the migration of significant amounts of silica and alkalis into solutions at any acidity at high *P–T* parameters. The formation of metamorphic fluids enriched in Fe, Mg, and Ca can be provided by acidic initial solutions only at the expense of leaching of these elements from metamorphic rocks.

ACKNOWLEDGMENTS

The authors thank L.Ya. Aranovich for stimulating discussion, D.V. Dolivo-Dobrovol'skii for the modification of the program complex FLUID, and an anonymous reviewer for valuable comments.

This study was financially supported by the Russian Foundation for Basic Research, project nos. 01-05-65174, 02-05-64803, and 07-05-00767; grant nos. MK-999.2003.05 and NSh-615.2003.5 of the Ministry of Industry and Science of the Russian Federation; grant nos. Y1-G-15-04 of the BRHE Program; and the Foundation for the Support of Russian Science.

REFERENCES

1. H. P. Eugster, "Minerals in Hot Water," Am. Mineral. **71**, (5–6) 655–673 (1986).
2. H. P. Eugster and W. D. Gunter, "The Compositions of Supercritical Metamorphic Solutions," Bull. Mineral. **104** (6), 817–826 (1981).
3. H. P. Eugster and L. Baumgartner, "Mineral Solubilities and Speciation in Supercritical Metamorphic Fluids," in *Thermodynamic Modeling of Geologic Materials: Minerals, Fluids and Melts*, Ed. by I. S. E. Carmichael and H. P. Eugster, Rev. Mineral. **17**, 367–403 (1987).
4. J. M. Ferry and D. M. Burt, "Characterization of Metamorphic Fluid Composition through Mineral Equilibria," in *Characterization of Metamorphism through Mineral Equilibria*, ed. by J. M. Ferry, Rev. Mineral. **10**, 207–262 (1982).
5. A. L. Skvirskii, S. A. Bushmin, A. S. Presnyak, and A. O. Petrochuk, "Thermodynamic Modeling of Interaction between Fluids and Minerals in Natural Multisystems," Zap. Vseross. Mineral. O-va **122**, 56–67 (1993).
6. A. L. Skvirski and S. A. Bushmin, "The Gibbs Free Energy Minimization Modeling Code for Computation of Fluid–Rock Equilibria in Geochemical Systems: 'FLUID' PC-Software Package," in *Models and Modeling of Geological Processes and Objects*, Ed. by V. Glebovitsky (Theophrastus, St. Petersburg–Athens, 2000), pp. 182–185.
7. D. V. Grichuk, *Thermodynamic Models of Submarine Hydrothermal Systems* (Nauchnyi mir, Moscow, 2000) [in Russian].
8. L. Haar, J. Gallagher, and G. Kell, "Thermodynamic Properties of Fluid Water," in *Proceedings of 9th International Conference on the Properties of Steam*, (New York, Pergamon, 1980), pp. 69–82.
9. J. C. Tanger IV and H. C. Helgeson, "Calculation of the Thermodynamic and Transport Properties of Aqueous Species at High Pressures and Temperatures: Revised

Equations of State for Standard Partial Molal Properties of Ions and Electrolytes," Am. J. Sci. **288** (1), 19–98 (1988).

10. D. A. Sverjensky, "Calculation of the Thermodynamic Properties of Aqueous Species and the Solubilities of Minerals in Supercritical Electrolyte Solutions," in *Thermodynamic Modeling of Geologic Materials: Minerals, Fluids and Melts*, Ed. by I. S. E. Carmichael and H. P. Eugster, Rev. Mineral. **17**, 177–209 (1987).
11. T. J. Holland and R. Powell, "An Internally-Consistent Thermodynamic Data Set for Phases of Petrological Interest," J. Metamorph. Geol. **16** (3), 309–343 (1998).
12. M. V. Borisov and Yu. V. Shvarov, *Thermodynamics of Geochemical Processes* (Mosk. Gos. Univ., Moscow, 1992) [in Russian].
13. GEOPIG (Group Exploring Organic Processes in Geochemistry): http://geopig.asu.edu/index.html
14. V. A. Pokrovskii and H. C. Helgeson, "Thermodynamic Properties of Aqueous Species and the Solubilities of Minerals at High Pressures and Temperatures: The System Al_2O_3–H_2O–NaCl," Am. J. Sci. **295** (10), 1255–1342 (1995).
15. S. Salvi, G. S. Pokrovski, and J. Schott, "Experimental Investigation of Aluminium–Silica Aqueous Complexing at 300°C," Chem. Geol. **151** (1–4), 51–67 (1998).
16. V. A. Pokrovskii, "Calculation of the Standard Partial Molal Thermodynamic Properties and Dissociation Constants of Aqueous $HC1^0$ and HBr^0 at Temperatures to 1000°C and Pressures to 5 kbar," Geochim. Cosmochim. Acta **63** (7–8), 1107–1115 (1999).
17. V. A. Pokrovskii and H. C. Helgeson, "Calculation of the Standard Partial Molal Thermodynamic Properties of KC1° and Activity Coefficients of Aqueous KCl^0 at Temperatures and Pressures to 1000°C and 5 kbar," Geochim. Cosmochim. Acta **61** (11), 2175–2183 (1997).
18. N. I. Khitarov, "The 400°C Isotherm for the System H_2O–SiO_2 at Pressures up to 4000 kg/cm^2," Geokhimiya, No. 1, 62–66 (1956) [Geochem. Int. No. 1, 55–61 (1956).
19. D. F. Weill and W. S. Fyfe, "The Solubility of Quartz in H_2O in the Range 1000–4000 bars and 400–550°C," Geochim. Cosmochim. Acta **28** (8), 1243–1255 (1964).
20. G. M. Anderson and C. W. Burnham, "The Solubility of Quartz in Supercritical Water," Am. J. Sci. **263** (6), 494–511 (1965).
21. G. M. Anderson and C. W. Burnham, "Reactions of Quartz and Corundum with Aqueous Chloride and Hydroxide Solutions at High Temperatures and Pressures," Am. J. Sci. **265** (1), 12–27 (1967).
22. R. A. Sommerfeld, "Quartz Solution Reaction: 400°–500°C, 1000 Bars," J. Geophys. Res. **72** (16), 4253–4257 (1967).
23. P. G. Novgorodov, "Solubility of Quartz in H_2O–CO_2 mixtures at 700°C and Pressures of 3 and 5 kbar," Geokhimiya, No. 10, 1484–1489 (1975) [Geochem. Int. **12**, 122–126 (1975)].
24. P. G. Novgorodov, "On the Solubility of Quartz in Mixtures $H_2O + CO_2$ and H_2O + NaCl at 700°C and 1.5 kbar Pressure," Geokhimiya, No. 8, 1270–1273 (1977) [Geochem. Int. **14**, 191–193 (1977)].
25. J. J. Hemley, J. W. Montoya, J. W. Marinenko, and R. W. Luce, "Equilibria in the System Al_2O_3–SiO_2–H_2O and Some General Implications for Alteration/Mineralization Processes," Econ. Geol. **75** (2), 210–228 (1980).
26. J. V. Walther and P. M. Orville, "The Extraction–Quench Technique for Determination of the Thermodynamic Properties of Solute Complexes: Application to Quartz Solubility in Fluid Mixtures," Am. Mineral. **68** (7–8), 731–741 (1983).
27. V. A. Sinitsyn and I. P. Ivanov, "Experimental Study of Aegirine Hydrolysis in NaOH Solutions," Dokl. Akad. Nauk SSSR **275** (5), 1172–1175 (1984).
28. S. W. Adcock, "The Solubility of Some Aluminosilicate Minerals in Supercritical Water—An Experimental and Thermodynamic Study," Ph.D. dissertation (Carleton University, Carleton, 1985).
29. C. E. Manning, "The Solubility of Quartz in H_2O in the Lower Crust and Upper Mantle," Geochim. Cosmochim. Acta **58** (22), 4831–4839 (1994).
30. I. P. Ivanov and N. A. Tkachenko, "Analysis of Mineral Assemblages and Modeling of Zoning of Acidic Metasomatites," in *Experimental and Theoretical Modeling of Mineral Formation*, Ed. by V. A. Zharikov and V. V. Fed'kin (Nauka, Moscow, 1998), pp. 173–188 [in Russian].
31. R. C. Newton and C. E. Manning, "Quartz solubility in H_2O–NaCl and H_2O–CO_2 Solutions at Deep Crust–Upper Mantle Pressures and Temperatures: 2–15 kbar and 500–900°C," Geochim. Cosmochim. Acta **64** (17), 2993–3005 (2000).
32. K. Shmulovich, C. Graham, and B. W. D. Yardley, "Quartz, Albite and Diopside Solubilities in H_2O–NaCl and H_2O–CO_2 Fluids at 0.5–0.9 GPa," Contrib. Mineral. Petrol. **141** (1), 95–108 (2001).
33. G. W. Morey, "The Solubility of Solids in Gases," Econ. Geol. **52** (3), 225–251 (1957).
34. I. G. Ganeev and V. N. Rumyantsev, "Solubility of Corundum in Water at High Temperatures and Pressures," Geokhimiya, No. 9, 1402–1403 (1974).
35. K. H. Becker, L. Cemič, and K. E. O. E. Langer, "Solubility of Corundum in Supercritical Water," Geochim. Cosmochim. Acta **47** (9), 1573–1578 (1983).
36. K. V. Ragnarsdottir and J. V. Walther, "Experimental Determination of Corundum Solubilities in Pure Water between 400–700°C and 1–3 kbar," Geochim. Cosmochim. Acta **49** (10), 2109–2115 (1985).
37. M. L. Pascal and G. M. Anderson, "Speciation of Al, Si, and K in Supercritical Solutions: Experimental Study and Interpretation," Geochim. Cosmochim. Acta **53** (8), 1843–1855 (1989).
38. J. V. Walther, "Experimental Determination and Interpretation of the Solubility of Corundum in H_2O between 350 and 600°C from 0.5 to 2.2 kbar," Geochim. Cosmochim. Acta **61** (23), 4955–4964 (1997).
39. B. Tagirov and J. Schott "Aluminum Speciation in Crustal Fluids Revisited," Geochim. Cosmochim. Acta **65** (21), 3965–3992 (2001).
40. E. L. Shock, D. C. Sassani, M. Willis, and D. A. Sverjensky, "Inorganic Species in Geologic Fluids: Correlations among Standard Molal Thermodynamic Properties of Aqueous Ions and Hydroxide Complexes," Geochim. Cosmochim. Acta **61** (5), 907–950 (1997).
41. G. C. Brown and W. S. Fyfe, "Kyanite–Andalusite Equilibrium," Contrib. Mineral. Petrol. **33** (3), 227–231 (1971).

42. A. F. Red'kin and T. K. Chevychelova, "Refinement of Some Mineral Equilibria and Compositions of Coexisting Solution in the System Al_2O_3–SiO_2–H_2O and 0.01 m HCl at 250–430°C and P = 1 kbar," Och. Fiz.-Khim. Petrol. **17**, (65–71) 1991.
43. G. T. Ostapenko and M. A. Arapova, "Solubility of Andalusite and Sillimanite in Water at 420–500°C and 1300 bar and Their Thermodynamic Constants," Geokhimiya, No. 11, 1297–1303 (1971).
44. G. T. Ostapenko, L. P. Timoshkova, and S. N. Tsymbal, "Gibbs Energy of Sillimanite from Data on Its Solubility in Water at 530°C and 1300 bar," Zap. Vses. Mineral. O-va **106**, 243–244 (1977).
45. G. W. Morey and J. M. Hesselgesser, "The Solubility of Some Minerals in Superheated Steam at High Pressures," Econ. Geol. **46** (8), 821–835 (1951).
46. C. J. Spengler and C. W. Burnham, "Compositions in the Upper Three Phase Region of the System $KAlSi_3O_8$–H_2O at Pressures up to 6 Kilobars," Geol. Soc. Amer. Spec. Pap., No. 68, 277 (1961).
47. K. L. Currie, "On the Solubility of Albite in Supercritical Water in the Range 400 to 600°C," Am. J. Sci. **266** (5), 321–341 (1968).
48. J. B. Adams, "Differential Solution of Plagioclase in Supercritical Water," Am. Mineral. **53** (9–10), 1603–1613 (1968).
49. G. M. Anderson and C. W. Burnham, "Feldspar Solubility and the Transport of Aluminium under Metamorphic Conditions," Am. J. Sci. **283A**, 283–297 (1983).
50. A. B. Woodland and J. V. Walther, "Experimental Determination of the Solubility of the Assemblage Paragonite, Albite, and Quartz in Supercritical H_2O," Geochim. Cosmochim. Acta **51** (2), 365–372 (1987).
51. G. M. Anderson, M. K. Pascal, and J. Rao, "Aluminium Speciation in Metamorphic Fluids," in *Chemical Transport in Metasomatic Processes*, Ed. by H. C. Helgeson, NATO ASI Ser. C (Math. and Phys. Sci.) (D. Reidel Publ., Dordrecht, 1987), Vol. 218, pp. 297–321.
52. J. V. Walther and A. B. Woodland, "Experimental Determination and Interpretation of the Solubility of the Assemblage Microcline, Muscovite, and Quartz in Supercritical H_2O," Geochim. Cosmochim. Acta **57** (11), 2431–2437 (1993).
53. P. Ya. Azimov and A. G. Shtukenberg, "Simulation of Phase Diagrams for Water–Salt Systems with Solid Solutions," Zh. Neorg. Khim. **45** (8), 1424–1432 (2000) [Rus. J. Inorg. Chem. **45**, 1302–1309 (2000).
54. J. V. Walther, "Experimental Determination of Portlandite and Brucite Solubilities in Supercritical H_2O," Geochim. Cosmochim. Acta **50**, 733–739 (1986).
55. J. J. Hemley, J. W. Montoya, C. L. Christ, and P. B. Hostetler, "Mineral Equilibria in the MgO–SiO_2–H_2O System: I. Talc–Chrysotile–Forsterite–Brucite Stability Relations," Am. J. Sci. **277** (3), 322–351 (1977).
56. R. C. Newton and C. E. Manning, "Solubility of Enstatite + Forsterite in H_2O at Deep Crust/Upper Mantle Conditions: 4 to 15 kbar and 700 to 900°C," Geochim. Cosmochim. Acta **66** (23), 4165–4176 (2002).
57. O. Vidal and L. Durin, "Aluminium Mass Transfer and Diffusion in Water at 400–550°C, 2 kbar in the K_2O–Al_2O_3–SiO_2–H_2O System Driven by a Thermal Gradient or by a Variation of Temperature with Time," Mineral. Mag. **63** (5), 633–647 (1999).
58. D. A. Crerar, S. Wood, S. Brantley, and A. Bocarsky, "Chemical Controls on Solubility of Ore Forming Minerals in Hydrothermal Solutions," Can. Mineral. **23**, 333–352 (1985).
59. J. J. Hemley, G. L. Cygan, and W. M. D'Angelo, "Effect of Pressure on Mineral Solubilities under Hydrothermal Conditions," Geology **14**, 377–379 (1986).
60. I.-M. Chou and H. P. Eugster, "Solubility of Magnetite in supercritical chloride solutions," Am. J. Sci. **277** (10), 1296–1314 (1977).
61. N. Z. Boctor, R. K. Popp, and J. D. Frantz, "Mineral–Solution Equilibria. IV. Solubilities and the Thermodynamic Properties of $FeCl_2^0$ in the System Fe_2O_3–H_2–H_2O–HCl," Geochim. Cosmochim. Acta **44** (10), 1509–1518 (1980).
62. G. P. Zaraiskii, "On the Differential Mobility of Components during Experimental Diffusion Metasomatism," in *Problems of Physicochemical Petrology (State of Fluid and Solutions, Metasomatism, Ore Formation* (Nauka, Moscow, 1979), Vol. 2, pp. 118–144 [in Russian].
63. G. P. Zaraiskii, *Zoning and Conditions of Metasomatic Rock Formation* (Nauka, Moscow, 1989) [in Russian].
64. V. K. Purtov, G. M. Yatluk, and V. N. Anfilogov, "Proportions of Fe, Mg, Si, and Al in Chloride Solutions at 873 K and 101 MPa in Relation to Skarn Formation in Limestones," Dokl. Akad. Nauk SSSR **275** (11), 1003–1006 (1984).
65. A. M. Dymkin, V. K. Purtov, and G. M. Yatluk, "On the Migration Properties of Iron in High-Temperature Hydrothermal Solutions," Dokl. Akad. Nauk SSSR **274** (1), 179–182 (1984).
66. V. K. Purtov and G. M. Yatluk, *Geochemistry of Major Elements in Skarn-Forming Solutions* (Nauka, Moscow, 1987) [in Russian].
67. V. K. Purtov and G. M. Yatluk, "On the Mobilization of Iron and Magnesium by HCl and NaCl Solution from the Rocks and Rock-Forming Minerals at a Temperature of 600°C and a Pressure of 1000 kg/cm^2," Dokl. Akad. Nauk SSSR **262** (5), 1242–1245 (1982).
68. E. H. Oelkers and H. C. Helgeson, "Calculation of the Thermodynamic and Transport Properties of Aqueous Species at High Pressures and Temperatures: Aqueous Tracer Diffusion Coefficients of Ions to 1000°C and 5 kb," Geochim. Cosmochim. Acta **52** (11), 63–85 (1988).
69. G. P. Zaraiskii, Yu. B. Shapovalov, V. N. Balashov, et al., "Experimental Study of Zoning and Formation Conditions of Ore-Bearing Metasomatites of the Acid Leaching Stage," in *Experiment and Solution of Important Geological Problems*, Ed. by V. A. Zharikov and V. V. Fed'kin (Nauka, Moscow, 1986), pp. 250–278 [in Russian].
70. V. A. Glebovitskii and S. A. Bushmin, *Post-Migmatite Metasomatism* (Nauka, Leningrad, 1983) [in Russian].
71. S. A. Bushmin, "Mineral Facies of Metasomatites Related to Regional Metamorphism," Zap. Vses. Mineral. O-va, **116**, 585–601 (1987).
72. S. A. Bushmin, L. V. Kuleshevich, and V. V. Severin, "Metasomatic Facies in the Eastern Baltic Shield," in *Metamorphic Facies of the Eastern Baltic Shield* (Nauka, Leningrad, 1990), pp. 87–118 [in Russian].

73. J. J. Wilkinson, J. Nolan, and A. H. Rankin, "Silicothermal Fluid: A Novel Medium for Mass Transport in the Lithosphere," Geology **24** (12), 1059–1062 (1996).

74. V. A. Glebovitskii, T. F. Zinger, I. K. Kozakov, et al., *Migmatization and Granite Formation under Different Thermodynamic Conditions* (Nauka, Leningrad, 1985) [in Russian].

75. S. P. Korikovskii, "Evolution of Zoned Metamorphic Complexes at Prograde and Retrograde Stages," in *Characteristics of Metamagmatism, Metasomatism, and Metamorphism*, Ed. by D. S. Korzhinskii, L. L. Perchuk, and N. N. Pertsev (Nauka, Moscow, 1987), pp. 160–188 [in Russian].

76. I. S. Sedova and V. A. Glebovitskii, "Features of Late Archean Granitization and Migmatization in the Belomorian Belt," Zap. Vseross. Mineral. O-va **134**, 1–24 (2005).

77. G. P. Zaraiskii, "The Conditions of the Nonequilibrium Silicification of Rocks and Quartz Vein Formation during Acidic Metasomatism," Geol. Rudn. Mestorozhd **41**, 294–307 (1999) [Geol. Ore Dep. **41** (4), 262–275 (1999)].

78. D. S. Korzhinskii, "An Outline of Metasomatic Processes," in *Fundamental Problems of Magmatic Ore Deposits* (Akad. Nauk SSSR, Moscow, 1955), pp. 334–456 [in Russian].

79. N. G. Sudovikov, *Regional Metamorphism and Some Petrological Problems* (Leningr. Gos. Univ., Leningrad, 1964) [in Russian].

80. A. M. Larin, D. V. Rundqvist, and E. Yu. Rytsk, "Evolution Trends of Geodynamic Environments and the Duration of Mineral Deposits Formation," in *Geodynamics and Metallogeny: Theory and Implications for Applied Geology*, Ed. by I. N. Mezhelovsky, A. F. Morozov, G. S. Gusev, and V. S. Popov (GEOKART, Moscow, 2000), pp. 193–212.

81. P. Kodera, A. H. Rankin, and J. Lexa, "Evolution of Fluids Responsible for Iron Skarn Mineralisation: An Example from the Vyhne-Klokoc Deposit, Western Carpathians, Slovakia," Mineral. Petrol. **64** (1–4), 119–147 (1998).

82. N. N. Pertsev and A. L. Kulakovskii, *Ferruginous Complex of the Central Aldan: Polymetamorphism and Structural Evolution* (Nauka, Moscow, 1988) [in Russian].

83. N. A. Eliseev, A. P. Nikol'skii, and V. G. Kushev, *Metasomatites of the Kriovi Rog Ore Belt* (Akad. Nauk SSSR, Moscow, 1961) [in Russian].

84. Yu. Ir. Polovinkina, "Sodium Metasomatism as a Regularity in the Formation of BIF Deposits," Zap. Vses. Mineral. O-va **78**, 52–58 (1949).

85. P. Ya. Azimov and A. G. Shtukenberg, "Thermodynamic Analysis of Factors Determining Growth Zoning in Metamorphic Garnets," Dokl. Akad. Nauk **376** (1), 235–237 (2001) [Dokl. Earth Sci. **376**, 79–80 (2001)].